Enhanced Land Subsidence Interpolation through a Hybrid Deep Convolutional Neural Network and InSAR Time Series

Zahra Azarm[1]; Hamid Mehrabi[1]; Saeed Nadi[2]

[1] Department of Geomatics Engineering, Faculty of Civil Engineering and Transportation, University of Isfahan, Isfahan, Iran

[2] Department of Civil an Environmental Engineering, Carleton University, Ottawa, Canada

Correspondence to: Hamid Mehrabi (h.mehrabi@eng.ui.ac.ir)

Abstract- Land subsidence, gradual or sudden ~~sinking of the land~~, poses a significant global threat to infrastructure and the environment. This ~~paper introduced~~study introduces a hybrid ~~method based on~~approach that combines deep convolutional neural networks (CNN) ~~and~~with persistent ~~scattered~~scatterer interferometric synthetic aperture radar (PSInSAR) to estimate land subsidence in areas where PSInSAR ~~cannot provide reliable measurements. This approach involves training~~data are unreliable or sparse. The proposed method trains a deep CNN ~~with~~using subsidence driving forces and PSInSAR data to learn spatial patterns and ~~estimate~~predict subsidence values. Our evaluation ~~of the model shows its efficiency in overcoming the~~demonstrates that the CNN effectively mitigates discontinuities ~~observed~~ in ~~the~~ PSInSAR results, producing a continuous and reliable subsidence surface. The ~~deep CNN~~model's performance was ~~evaluated on~~assessed using training, validation, and testing ~~data, resulting in~~datasets, achieving root mean ~~squared~~square errors (RMSE) of ~~5~~3.99 mm, 8.47 mm, and 9 mm, ~~and 11 mm,~~ respectively. In contrast, ~~the kriging~~traditional interpolation ~~method showed a mean square error of 37.19 mm in the experimental data set. subsidence prediction using the deep CNN method showed a 70% improvement compared to the~~methods such as Kriging, inverse distance weighting (IDW), and radial basis function (RBF) interpolation ~~method.~~ yielded RMSE

Style Definition: Normal (Web)

Formatted: Font: 10 pt

Formatted: Footnote Text

Formatted: English (United States)

values of 61.60 mm, 66.21 mm, and 61.76 mm, respectively, on the test dataset. Additionally, the coefficient of determination (R^2) for CNN, Kriging, IDW, and RBF was 0.98, -0.06, -0.22, and -0.06, respectively. The deep CNN model demonstrated an 85% improvement in subsidence prediction accuracy compared to conventional interpolation methods, highlighting its potential for accurate and continuous land subsidence estimation.

***Index Terms*— Convolutional Neural Network (CNN); Prediction of subsidence; PSInSAR; driving forces; Kriging interpolation.**

1. Introduction

The gradual decrease in the height of the earth's surface, which is accompanied by slight horizontal displacements, is called subsidence. Due to the gradual nature of land subsidence, this phenomenon is also called "silent earthquake". Its harmful effects appear over a long period of time and carry significant risks. However, land subsidence is a global threat to urban areas around the world (Sun et al., 2023). This issue is an important global concern and is not limited to one region. Iran is facing an increasing challenge especially in this field. Human activities, such as mining and excessive underground water extraction, contribute to this problem. To address it, effective groundwater management to prevent unauthorized water extraction would help. However, land subsidence is not only caused by human actions, natural factors also play an important role. These include water table fluctuations, soil characteristics, depth of the bed rock, terrain features like elevation and aspect, vegetation cover, and prevailing climate. All these factors together create a complex landscape of land subsidence occurrences.

Precise leveling and GNSS observations offer high precision in measuring subsidence. Still, they are limited in their ability to investigate subsidence over a wide area due to their reliance on measuring sparse stations. These methods require multiple measurements at different locations, making it difficult to monitor subsidence over large areas (Fialko et al., 2005; Hu et al., 2012). On the other hand, Interferometric Synthetic Aperture Radar (InSAR), has emerged as a high spatial resolution and cost-effective technique for monitoring subsidence on a large scale (Chang et al., 2010; Tamburini et al., 2010; Tomás et al., 2011; Rucci et al., 2012; Amighpey & Arabi, 2016; Biswas et al., 2018; Gonnuru & Kumar, 2018; Khorrami et al., 2019). InSAR uses radar waves to carefully monitor changes in the Earth's crust surface over time. Methods that analyse radar images over time, known as time series analysis, make them very effective for monitoring subsidence, which usually occurs gradually over time. Persistent Scatterer Interferometric Synthetic Aperture Radar (PSInSAR) is particularly valuable for monitoring urban land subsidence. This is because

there are many high-density Persistent Scatterer (PS) points, mainly associated with buildings and man-made structures. This abundance significantly improves the quality of the data within interferograms (Gao et al., 2019). Although these advantages are significant, dealing with the sparse and uneven distribution of PSs in both spatial and temporal dimensions is a significant computational challenge. The PSInSAR approach generates discontinuous results, as it calculates subsidence exclusively at PS points. Consequently, it becomes imperative to employ intelligent interpolation instead of mathematical or stochastic methods, between these data points to fill out these gaps (Naghibi et al., 2022).

Subsidence is a complex physical phenomenon influenced by a multitude of factors, such as changes in groundwater levels, soil type, bedrock depth, slope, elevation, Aspect, etc. To obtain the subsidence in the whole area, interpolation methods between PSs and artificial intelligence methods (which are trained with features affecting subsidence) can be used. Interpolation methods between PSs and artificial intelligence methods (trained with features affecting subsidence) can be used to obtain subsidence in the entire area. Classical interpolation methods (e.g. Kriging, IDW, RBF (Mehrabi & Voosoghi, 2018), RMLS (Mehrabi & Voosoghi, 2015)) do not consider the physics of the issue, making their results less reliable. So, it is very important to apply methods that take into account the real characteristics of the phenomenon, especially when monitoring the subsidence. Recently, machine learning methods specifically deep convolutional neural network (CNN) shows encouraging results in various applications. In the larger context of land subsidence prediction models, we find two main categories: Physical Process Models: These models simulate subsidence by incorporating factors like geotechnical mechanics, soil properties, and water dynamics. They are frequently used in large-scale projects but require a substantial amount of prior knowledge and data (Nie et al., 2015); Mathematical or Statistical Models: These models predict subsidence based on historical elevation data and past trends (Zhu et al., 2010).

Several studies have investigated various forecasting models, methodologies, and influencing factors to improve our understanding of this field. Neural networks have emerged as powerful prediction tools, so neural networks have been used in the field of subsidence prediction using its driving forces. (Zhu et al., 2010; Azarakhsh et al., 2022; Ku & Liu, 2023). Lee et al. (2023) employed data from an urban area in Korea to develop a machine learning-based model for predicting land subsidence risk. Their methodology incorporated historical land subsidence data along with attribute information pertaining to underground utility lines in the specified region. The research team utilized machine learning algorithms such as Random Forest (RF), eXtreme Gradient Boosting (XGBoost), and Light Gradient Boosting Machine (LightGBM) for the analysis and prediction of land subsidence risks (Lee et al., 2023). Sadeghi et al. (2023)

Formatted: Font: Not Italic

combined full consistency decision-making (FUCOM) and GIS methodologies to assess Iran's vulnerability to land subsidence. Their approach resulted in the development of a hierarchical FUCOM-GIS framework, which highlighted critical factors such as water stress, groundwater depletion, soil type, geological time scale, and rainfall amount as the main drivers of land subsidence. Researchers commonly validate their results by comparing them with InSAR analyses, identifying areas exhibiting notable subsidence. Furthermore, the research assessed the risks to power transmission lines and substations, revealing structural issues such as pier sinking, electric insulator deviation, and cracking(Sadeghi et al., 2023). In another study focused on Dechen County, China, Wang et al. (2023) employed Backpropagation Neural Network (BPNN) and RF algorithms, in conjunction with various monitoring data sources, GIS, and SBAS technology, to predict trends in land subsidence. Their findings underscored Sugianto town as the most severely affected area, with an annual average subsidence rate of -40.71 mm per year. The study highlighted that changes in both deep and shallow groundwater levels were the primary drivers of land subsidence in this region. Notably, the BPNN model demonstrated higher prediction accuracy compared to the RF model, especially when considering changes in groundwater levels (Wang et al., 2023). Furthermore, Zhuo et al. (2020) demonstrated that the integration of the GM (1,3) model with neural networks and ground-related variables shows great potential for achieving highly accurate subsidence predictions. The proposed approach has the capability to replace traditional precise leveling methods in long-term subsidence forecasting, offering valuable insights for urban disaster prevention (Zhou et al., 2020).

Deng et al. (2017) conducted research on the integration of PSInSAR with Grey system theory for monitoring and predicting land subsidence, as demonstrated in the Beijing plain (Deng et al., 2017). Precision mapping of complete subsidence basins faces challenges, especially when dealing with image pairs with limited temporal separation. Rapid deformations and vegetative changes in such scenarios introduce complexity. Strategies, such as combining differential interferometric synthetic aperture radar (DInSAR) with the probability integral model (PIM), have been introduced to effectively delineate subsidence basins resulting from mining activities (Fan et al., 2015).

The remarkable effectiveness of the RF model in mapping the susceptibility of land subsidence deserves attention. This approach demonstrates exceptional capabilities in identifying key factors that contribute to subsidence occurrences, such as the proximity to faults, elevation, slope angle, land use patterns, and water table levels. These factors play a crucial role in influencing the likelihood of subsidence events (Mohammady et al., 2019). In addition, the integration of fuzzy logic techniques and neural networks has been used to predict subsidence (Ghorbanzadeh et al., 2020).

Land subsidence is a significant geological risk and predicting and investigating this phenomenon is vital. Traditional monitoring and forecasting methods have limitations and require more advanced approaches. Kumar et al. (2022) utilize recurrent neural networks (RNNs), specifically Vanilla and Stacked Long Short-Term Memory (LSTM) models, to forecast land subsidence in the Jharia Coalfield, Dhanbad, India. Using data from 14 locations collected through the Modified PSInSAR technique, the study shows these models can effectively predict deformation rates, identifying critical subsidence levels at Nai-dunia basti, Digwadih, and Godhar. This research underscores the potential of integrating advanced monitoring techniques with sophisticated predictive models to better anticipate and mitigate land subsidence impacts (Kumar et al., 2022).

The integration of InSAR processing with deep learning methods in modeling and predicting land subsidence has shown significant promise. This approach demonstrates substantial capabilities in identifying and predicting subsidence in regions around Lake Urmia by leveraging Sentinel-1 data and small baseline subsets (SBAS) InSAR methods. Key factors such as rainfall, groundwater levels, and lake area variations, measured using TRMM, GRACE, and MODIS satellite data, were critical in understanding subsidence dynamics. Moreover, the application of machine learning models, including multi-layer perceptron (MLP), convolutional neural network (CNN), and long short-term memory (LSTM) networks, has been instrumental in improving prediction accuracy. The ensemble model combining these networks outperformed individual models, achieving enhanced prediction reliability (Radman et al., 2021).

Predicting deformation is essential for early detection of abnormal conditions and timely intervention. A recent study introduced a deep convolutional neural network (DCNN) approach to forecast time-series deformation using InSAR data. The research, conducted at Hong Kong International Airport, demonstrated that the DCNN could effectively predict both linear land settlement and nonlinear thermal expansion of structures with high accuracy. The study's findings highlight the DCNN's potential to enhance early warning systems by providing precise short-term deformation predictions, thus enabling better risk management and mitigation strategies (Ma et al., 2020).

In this study we used a CNN model trained over the area where subsidence is available through PSInSAR. Then this model is used over other areas where subsidence cannot be obtained from PSInSAR processing. The proposed method follows three main steps: Calculation of subsidence in PSs by PSInSAR method, calculation of subsidence driving ~~factors~~forces, and training CNN.

2. Methodology

2.1 PSInSAR

PSInSAR is a remote sensing technique that utilizes SAR images to monitor surface deformation over time. It relies on identifying PSs, which are stable points on the Earth's surface reflecting radar signals consistently. PSInSAR combines multiple interferograms created by comparing SAR images of the same area taken at different times. By analysing phase differences between radar signals in these interferograms, it detects changes in the Earth's surface over time. PSInSAR has significant advantages over DInSAR, as it effectively eliminates topographic errors, atmospheric noise, and addresses temporal and spatial correlation issues between radar images (Ferretti et al., 2001; Wasowski & Bovenga, 2014; Gonnuru & Kumar, 2018). PSInSAR, a form of differential interferometry, involves analysing a collection of at least 15 SAR images captured at different times, all covering the same area (Crosetto et al., 2016). PSInSAR finds diverse applications, including monitoring subsidence in urban areas (Ferretti et al., 2000; Luo et al., 2013) and tracking natural hazards such as landslides, earthquakes, and volcanic activity (Peltier et al., 2010). However, one drawback of PSInSAR is the lack of continuity between PSs, as they depend on the land use of the area. These PSs are more abundant in areas with buildings, dams, oil wells, pipelines, electric fences, roads, rocks, and bridges (Din et al., 2015), but they are relatively scarce in vegetated areas. Consequently, PSInSAR performs best in urban areas and regions with rocky terrain (Oštir & Komac, 2007).

In this article, the amplitude dispersion index is used to select the persistent scatterer points, Eq. (1). The usual threshold of the amplitude dispersion index is limited between 0.2 and 0.4 (Conway, 2016).

$$D_A = \sigma_A / \mu_A \tag{1}$$

where μ_A , σ_A are standard deviation and mean values of the radiometrically corrected amplitude of pixels. In PSInSAR the amplitude data from SAR images is carefully examined to identify specific PSs while excluding those affected by space-time decoherence and atmospheric delay (Li et al., 2004).

2.2. Deep Convolutional neural network (CNN)

~~CNN is a type of~~CNNs, or Convolutional Neural Networks, are deep learning ~~algorithm~~algorithms widely employed for various image-related tasks ~~like~~such as image recognition, classification, and regression. ~~CNNs can automatically~~ They learn and extract essential features from raw ~~image. They accomplish this~~ images by processing ~~images~~them through multiple layers of filters, known as "convolutions~~," which~~." This multi-layer processing progressively

~~extract~~extracts more abstract features. These filters are trained using backpropagation, a technique that adjusts filter weights based on the difference between predicted and actual outputs. In addition to convolutional layers, CNN typically includes pooling layers to down sample the convolutional output and fully connected layers to use the extracted features for image classification. CNN has gained popularity, particularly after the success of AlexNet in the ImageNet challenge in 2012 and has since become the dominant approach for image recognition tasks.

CNN is used in various fields, including medical imagery (Lee et al., 2017), classification (LeCun & Bengio, 1995), segmentation (Nair & Hinton, 2010; Van Do et al., 2024), image reconstruction (Christ et al., 2016; Lakhani & Sundaram, 2017; Elboushaki et al., 2020), and natural language processing (Kim et al., 2018). While CNN are often associated with categorical tasks, they are also highly effective in regression tasks, where the goal is to predict continuous output variables instead of discrete labels. In CNN regression, the network typically has a single output neuron in the final layer that generates a continuous value instead of a probability distribution for classification. It is important to note that CNN requires a lot of input data, especially for image processing. As the network's depth increases, so does its complexity, resulting in a larger number of weight parameters, which can sometimes create challenges during training (Liu et al., 2018). CNN introduced the concept of local connections between layers with typical components including convolution, activation and pooling layers (Chen et al., 2018). The convolutional layer learns image features from small sections of input data through mathematical operations involving the input image matrix and a filter or kernel. The activation layer introduces nonlinearity into the network, commonly using the Rectified Linear Unit (ReLU) function.

CNN regression is a valuable approach for predicting continuous output variables and has found applications in various fields including geology and civil engineering. CNN regression can also be used to predict subsidence. By training a CNN model with input-output pairs, where inputs are subsidence driving forces and outputs represent subsidence values, researchers can predict subsidence at single-pixel levels and provide valuable insights.

To predict land subsidence, we trained a CNN regression model with the architecture shown in **Error! Reference source not found.**. The CNN has 31 layers, including three 1×1 convolutional layers, three 3×3 convolutional layers followed by three 2×2 max-pooling layers, Batch Normalization layers, drop out layers with a rate of 0.1, and two fully-connected layers with 1024 Rectified Linear Unit (ReLU) activation neurons, two fully-connected layers with 512 ReLU activation neurons, and a fully-connected layer with 256 ReLU activation neurons. The input dimensions

are 30×30×9, where 30×30 patches separated from the neighborhood of each scattered point and 9 features are used as network input.

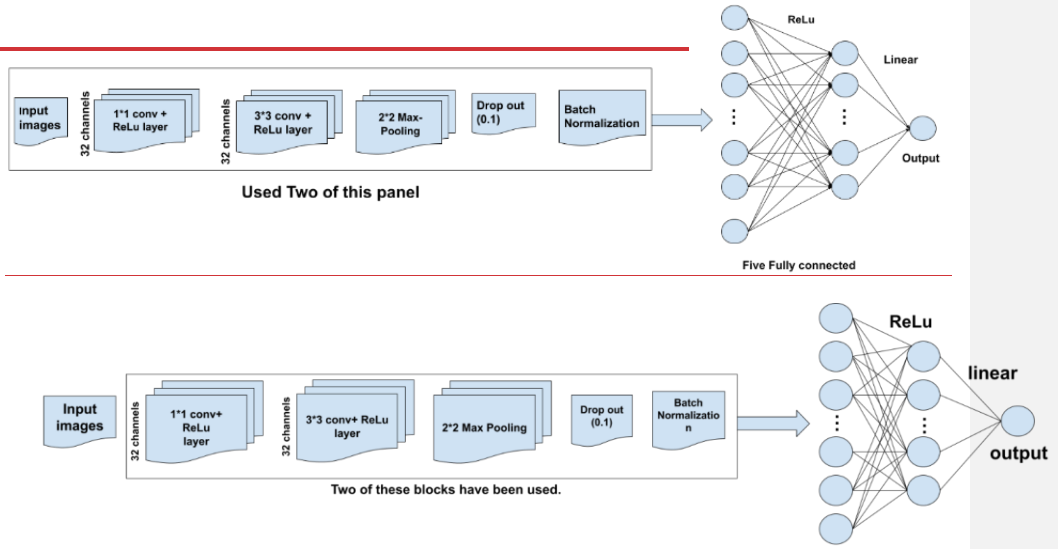

Figure ~~1:~~1: Illustration of CNN Architecture

Formatted: Line spacing: single

2.2.1. Hyperparameter Tuning Process

After creating the model architecture, model inputs were normalized to a range of [0, 1] to ensure consistent input scaling, which is crucial for the stable performance of the neural network. Then we tuned the hyperparameters of the CNN regression model, including the loss function, optimizer, batch size, learning rate, activation function, and number of epochs. The best model was saved based on its performance metrics. The rationale for each hyperparameter is explained in detail and the optimal parameters for the model are given in Table 1:

- **Activation function:** We used the ~~mean square error function~~Rectified Linear Activation (ReLU) function in the hidden layers due to its effectiveness in mitigating the vanishing gradient problem and promoting sparse activations. For the output layer, a Linear activation function was employed to ensure the model could predict a continuous range of values.

Formatted: English (United States)

- **Loss function:** We considered both Mean Squared Error (MSE) and Mean Absolute Error (MAE) as ~~the cost function, a batch size of~~ potential loss functions. MSE penalizes larger errors more heavily than MAE, making it suitable for scenarios where outliers significantly impact the model's performance. Given MSE's properties and its ability to improve the model's performance by reducing fluctuations and speeding up convergence, we selected MSE as our loss function. The MSE is calculated as follows:

$$MSE = {}^{1}/_{N} \sum_{i}^{N} (Y_i - \hat{Y}_i)^2 \quad (2)$$

where Y_i represents the actual values, $\hat{Y}_i$ represents the predicted values, and N is the number of observations.

- **Batch Size**: We experimented with batch sizes of 64 and 128~~, a~~. A larger batch size of 128 was chosen as it provided a good balance between training speed and model performance, allowing more stable gradient estimates.
- **Learning Rate**: The initial learning rate was set to 0.001, but we found that a smaller learning rate of 0.0001, led to more gradual and ~~trained~~stable convergence, reducing the ~~network~~risk of overshooting the optimal solution.
- **Optimizer**: The Adam optimizer was selected for its adaptive learning rate capabilities and efficiency in handling sparse gradients. It combines the advantages of both the AdaGrad (Adaptive Gradient Algorithm) and RMSProp (Root Mean Square Propagation) algorithms, making it suitable for our regression task.
- **Number of Epochs**: We initially set 100 epochs but extended this to 150 epochs~~.~~ to ensure the model had sufficient time to learn the underlying patterns in the data without overfitting.
- **To divide the data**~~:~~, we initially allocated 15% to the test data, 15% to the validation data, and 70% to the training data. However, we ~~noticed~~observed high-cost function fluctuations ~~for~~in the training and validation data~~, so~~. To mitigate this issue, we ~~increased~~adjusted the ~~training~~ data split to 80~~%,~~ % for training and ~~allocated~~ 10% each ~~to the test~~for testing and validation ~~data. This~~, which helped ~~to~~ reduce the fluctuations ~~(Table 1)~~.

Table 1. Key parameters of the CNN

parameters	value

Formatted: English (United States)

Formatted: English (United States)

Formatted: English (United States)

Formatted: English (United States)

Formatted: English (United States)

Formatted: English (United States)

Formatted: Font: Bold, English (United States)

Formatted: English (United States)

Formatted: English (United States)

Formatted: Outline numbered + Level: 1 + Numbering Style: Bullet + Aligned at: 0.25" + Tab after: 0.5" + Indent at: 0.5"

Formatted: English (United States)

Formatted: English (United States)

Formatted: English (United States)

Formatted: English (United States)

Formatted: English (United States)

Formatted: English (United States)

Formatted: English (United States)

Formatted: English (United States)

Formatted: English (United States)

Formatted: English (United States)

Formatted: English (United States)

Formatted: English (United States), Highlight

Formatted: English (United States)

Formatted: Font: Bold

Formatted: Left

Activation function of hidden layer, input layer	ReLu
Activation function of output layer	Linear
Input shape	30×30×9
Loss function	MSE
Batch size	128
Learning rate	0.0001
Epoch	150
Train-validation-test	80% -10% -10% Of total data

Formatted: Left
Formatted: Left
Formatted Table
Formatted: Left
Formatted: Left
Formatted: Left
Formatted: Left
Formatted Table
Formatted: Left
Formatted: English (United States)

2.3. Driving forces of subsidence

~~Previous research in this field has identified several factors that impact land subsidence. These factors include changes in the water table, soil type, depth of the rock bed, elevation, slope, aspect, rainfall patterns, vegetation cover, flow index, topography index, distance from rivers, distance from faults, lithology~~The selected driving factors for predicting subsidence—NDVI, distance from wells, land use, water table map, altitude, slope, SPI, TWI, and aspect—are well-supported by extensive research and have been identified as significant predictors in previous studies (Yang et al., 2014; Fan et al., 2015; Conway, 2016; Abdollahi et al., 2019; Andaryani et al., 2019; Mohammady et al., 2019; Zang et al., 2019; Ghorbanzadeh et al., 2020; Shi et al., 2020; Zhou et al., 2020; Zhao et al., 2021; Wang et al., 2023). By incorporating these factors into the subsidence prediction model, this study ensures a comprehensive approach that reflects the complexity of subsidence phenomena.

Formatted: Body Text, Left, Line spacing: Double
Formatted: Font color: Auto
Formatted: Font color: Auto
Formatted: Font color: Auto

1. NDVI is a crucial indicator of vegetation health and land cover changes. Changes in NDVI can reflect alterations in land use practices, such as urbanization or agricultural expansion, which are closely linked to subsidence. Healthy vegetation typically reduces the need for excessive groundwater extraction, while barren or urbanized areas might correlate with higher subsidence due to increased groundwater use.

2. The distance from groundwater extraction wells is a critical factor in subsidence studies. Areas closer to high-density exploitation wells often experience more severe subsidence due to the localized impact of extensive groundwater withdrawal.

3. Land use changes, including urbanization, agricultural expansion, and deforestation, influence subsidence rates. Urban areas often experience higher subsidence due to increased groundwater extraction for residential, industrial, and agricultural purposes.

4. Groundwater level changes, as depicted in water table maps, are directly linked to subsidence. Over-extraction of groundwater leads to a drop in the water table, causing the ground to compact and subside nce. Groundwater depletion is a primary contributor to subsidence, emphasizing the importance of preventing unauthorized withdrawals and effectively managing water resources.

5. Altitude influences subsidence through its effect on hydrological processes. Altitude affects the distribution and movement of groundwater. Higher altitudes typically receive more precipitation, which can infiltrate the ground and recharge aquifers. At lower altitudes, reduced precipitation and higher evaporation rates can lead to a lowering of the water table. When groundwater is extracted faster than it is replenished, it can result in subsidence. The amount of water in the soil, influenced by altitude through precipitation and drainage patterns, affects soil compaction. High altitude areas with abundant rainfall can lead to saturated soils which are less prone to subsidence. Conversely, in lower altitude areas with less precipitation, soils may dry out and compact more easily, contributing to subsidence.

6. Slope affects water runoff and infiltration rates. Steeper slopes may reduce infiltration, leading to less groundwater recharge and potentially higher subsidence rates in adjacent flat areas.

7. Aspect affects solar radiation and, consequently, evaporation and soil moisture levels. Different aspects can lead to variations in vegetation cover and groundwater recharge, influencing subsidence. Additionally, the slope and aspect of an area can influence drainage patterns, erosion, and sediment production, all contributing to subsidence.

8. The Stream Power Index (SPI) measures the power of water flow in depositing and causing soil erosion. As a result, this index can be an important input for subsidence prediction models. The equation used to calculate SPI is as follows (Pradhan et al., 2014):

$$SPI = \alpha * \tan\beta \quad (4)$$

Here, α flow accumulation, and β represents the slope.

Formatted: List Paragraph, Numbered + Level: 1 + Numbering Style: 1, 2, 3, … + Start at: 1 + Alignment: Left + Aligned at: 0.25" + Indent at: 0.5"

Formatted: Indent: Before: 0.25", First line: 0.25"

9. The Topographic Wetness Index (TWI) is a mathematical formula that quantifies the effect of local topography on the flow of surface water. It is a physically based index that can be used to determine flow direction and accumulation and has many practical applications in fields such as hydrology, agriculture, and geology. TWI indicates areas of potential soil moisture accumulation. Areas with high TWI values are likely to have more groundwater recharge, which can mitigate subsidence.

In rainfall runoff modeling, TWI can be used to predict the amount and timing of runoff in a specific area, while in soil moisture modeling it can be used to predict the spatial distribution of soil moisture. Overall, the TWI is a useful tool for understanding and predicting the movement of water across the landscape (Qin et al., 2011). Also, TWI identifies areas that can be affected by flooding from rainfall events (Ballerine, 2017). TWI equation is as follows (Moore et al., 1991):

$$TWI = \ln(\alpha/\tan\beta) \quad (23)$$

~~Where α the upslope contributing area and β is slope. TWI is calculated utilizing a Digital Elevation Model (DEM) of the study areas. The flow power index~~Where α the upslope contributing area and β is slope. TWI is calculated utilizing a Digital Elevation Model (DEM) of the study areas.

~~1. (SPI) measures the power of water flow in depositing and causing soil erosion. As a result, this index can be an important input for subsidence prediction models. The equation used to calculate SPI is as follows (Pradhan et al., 2014):~~

$$SPI = \alpha * \tan\beta \quad (3)$$

~~Here, α flow accumulation, and β represents the slope.~~ ~~Land subsidence results from a combination of factors, including both topographic and altitude-related features, such as rainfall and lithology. Research has demonstrated that areas at lower altitudes tend to experience more subsidence. Additionally, the slope and aspect of an area can influence drainage patterns, erosion, and sediment production, all contributing to subsidence. The amount of vegetation, as measured by the Normalized Difference Vegetation Index (NDVI), also plays a significant role. Less vegetation often indicates a higher risk of subsidence. The distance from a river and distance from faults are other crucial subsidence driving forces. Groundwater depletion is a primary contributor to subsidence, emphasizing the importance of preventing unauthorized withdrawals and effectively managing water resources.~~ It's essential to recognize that examining one factor alone is not enough to predict subsidence. A linear relationship between groundwater level changes and subsidence may exist in certain regions, but this linear relationship does not exist in

Formatted: Indent: Before: 0.5"

Formatted: List Paragraph, Numbered + Level: 1 + Numbering Style: 1, 2, 3, … + Start at: 1 + Alignment: Left + Aligned at: 0.25" + Indent at: 0.5"

Formatted: Indent: Before: 0.25", First line: 0.25"

all regions. Each region has unique characteristics such as soil type, fault lines and slope, etc. Subsidence is a complex phenomenon that requires a comprehensive investigation that takes into account all relevant factors. Therefore, thorough analysis is necessary to obtain a comprehensive understanding of subsidence in a particular area (Azarm et al., 2023).

3. Study Area and Datasets

3.1. Study area

The studied area is in Isfahan province and includes the cities of Isfahan, Mahyar, Khomeinishahr and Falavarjan. This region has a rich history of human habitation, diverse cultural heritage and a wide range of economic activities. Covering approximately 7000 square kilometers, this area displays various uses, including urban, agricultural and industrial areas. Its climate is semi-arid, characterized by hot summers and cold winters. The primary sources of water in this area are the Zayandeh-Rud River and several underground aquifers that provide various uses such as agriculture, drinking water, and industrial needs (Neysiani et al., 2022) (Fig. 2). To effectively monitor and predict land subsidence in this study area, we used advanced techniques such as radar interferometry and convolutional neural networks (CNN). Our goal was to provide an accurate and reliable estimate of land subsidence in the study area by integrating these techniques and considering complex subsidence driving forces.

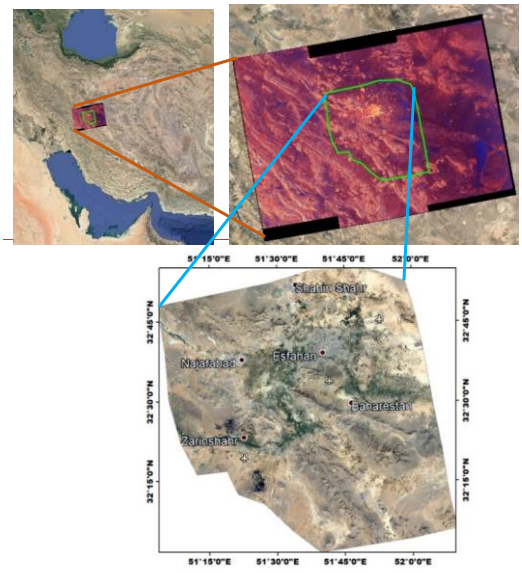

~~Figure 2: Geographic overview of the study area. (© Google Earth)~~

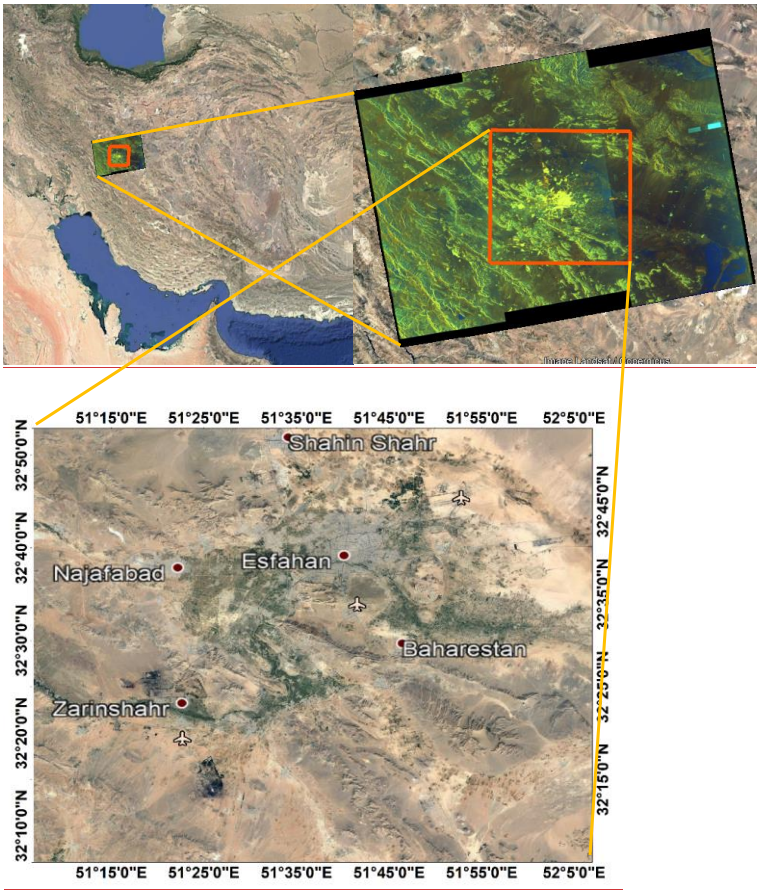

Figure 2: Geographic overview of the study area. (© Google Earth)

3.2. Datasets

3.2.1. Sentinel-1A Radar Images

This study ~~uses~~utilizes 73 radar images ~~obtained~~ from the Sentinel-1A satellite to ~~analyse~~analyze subsidence trends in the study area over a ~~six~~seven-year period, from 2014 to 2020. The data was collected from the Ascending track 28. The Sentinel-1A satellite, launched by the European Space Agency (ESA), operates in C-band and provides Synthetic Aperture Radar (SAR) imagery with a spatial resolution of 5 meters by 20 meters. The images were acquired at six-day intervals, ensuring high temporal resolution for detecting ground movements. The Interferometric Wide (IW) swath mode was used, offering comprehensive coverage of the study area.

Formatted: English (United States)
Formatted: English (United States)
Formatted: English (United States)
Formatted: English (United States)
Formatted: English (United States)
Formatted: English (United States)

The PSInSAR technique was applied to the Sentinel-1A data using ~~the~~ Sarproz software. ~~The 30 meters SRTM DEM~~ ~~of~~This method is particularly effective in urban and semi-urban areas where permanent scatterers are abundant. The precise processing steps involved coregistration, interferogram generation, phase unwrapping, and geocoding to produce detailed subsidence maps (Ferretti et al., 2001).

~~**the study area, with a spatial resolution of 30 meters, was used**~~**3.2.2. Digital Elevation Model (DEM)**

The 30-meter Shuttle Radar Topography Mission Digital Elevation Model (SRTM DEM) was employed to calculate ~~the~~various topographical and hydrological indices, including SPI, TWI, slope, and aspect. These indices were computed using ~~the~~ ArcMap software. ~~The obtained data provided~~ , providing essential insights into the terrain characteristics influencing subsidence ~~driving forces~~ (Fig. 3, Fig.4).

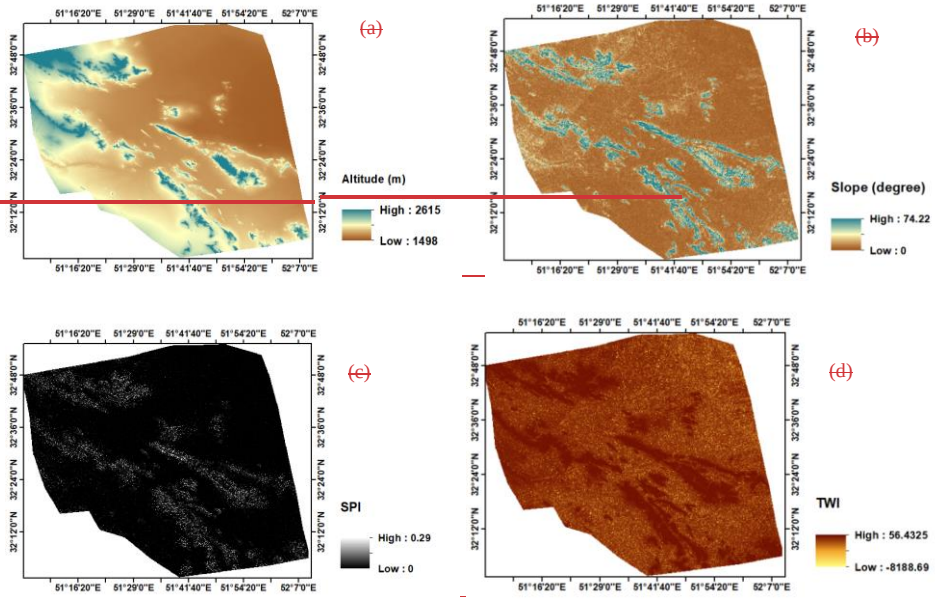

359

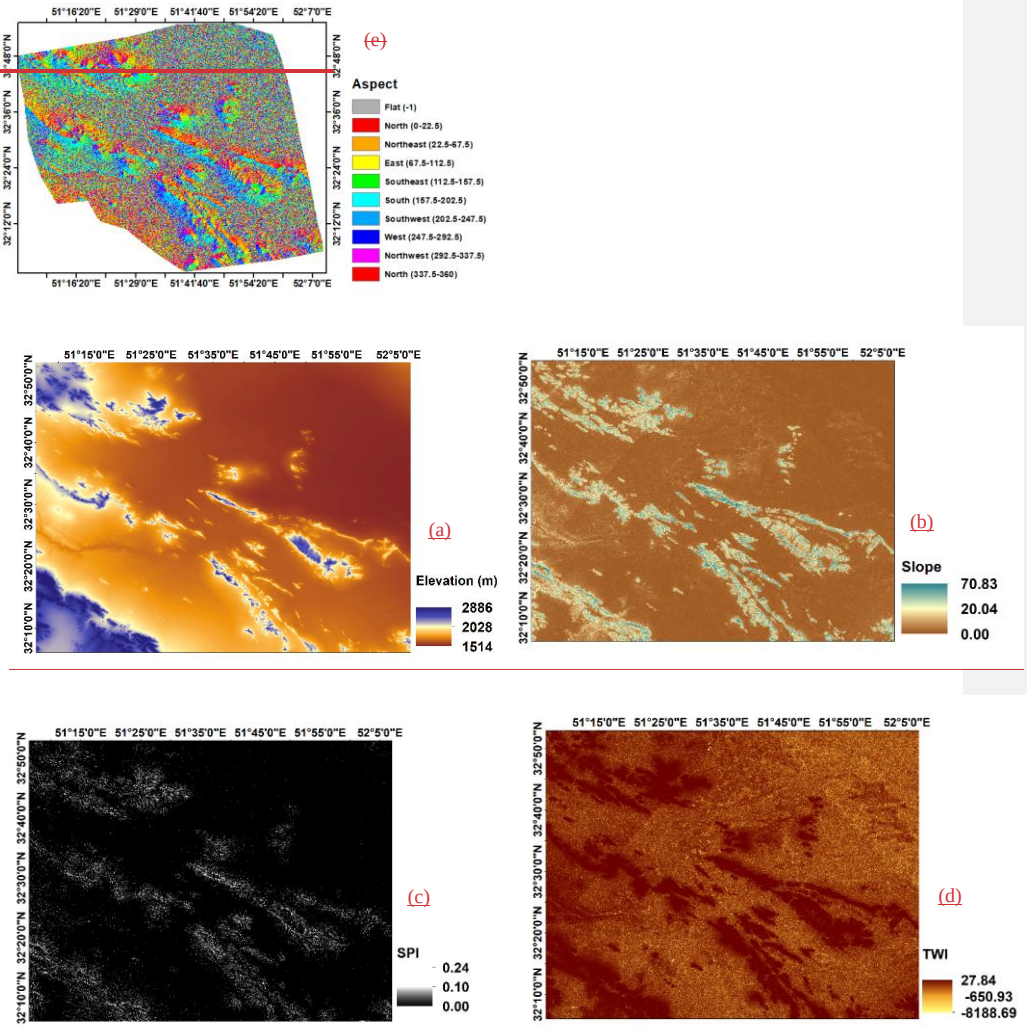

360 **Figure ~~3.~~3: Subsidence driving forces - (a) ~~Altitude~~Elevation, (b) Slope, (c) SPI, (d) TWI**

361

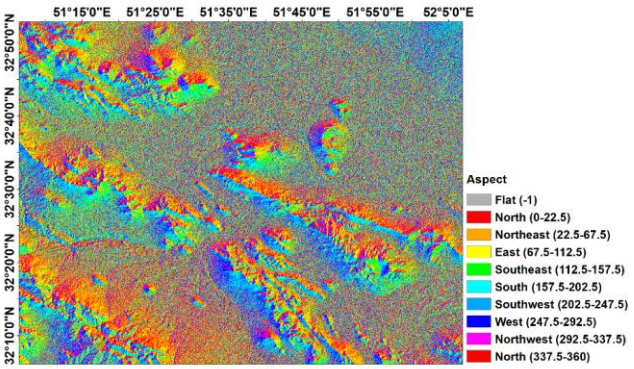

Figure 4: Subsidence driving force – (e) Aspect

Formatted: Left

~~The~~ 3.2.3. Optical Satellite Images

Optical images from the Landsat 8 satellite, launched by NASA ~~provided optical images that,~~ were used ~~in this study~~ to extract ~~the~~ NDVI and land use information ~~in the study area~~ for the year 2020. ~~Average~~The Landsat 8 images, with a spatial resolution of 30 meters, were processed using Envi software to calculate average annual changes ~~of~~in NDVI between 2014 and 2020 ~~were calculated with Envi software. The relationship between subsidence and groundwater~~ . This analysis helps in understanding the impact of vegetation and land use changes on subsidence (Fig. 5).

3.2.4. Groundwater Monitoring Data

Groundwater level changes ~~should be~~were investigated ~~over a long period of time. Therefore, in this research, using~~ ~~the~~ using data from piezometric wells ~~of the region, the~~within the study area. The groundwater monitoring data, covering the period from 2014 to 2020, were sourced from Isfahan Regional Water Authority. These data were collected monthly and provided detailed information on the groundwater table fluctuations. The data were processed to generate water table ~~map was calculated for the period of 2014 to 2018In areas where the density~~maps, which were then analysed in relation to subsidence patterns. In areas with high densities of exploitation wells ~~is higher due to the extraction of underground water resources~~, the probability of subsidence ~~is higher in those areas, so the~~increases due to significant groundwater extraction. The distance from ~~exploitation~~these wells was calculated and included as one of the driving forces for subsidence (Fig. ~~4~~5).

Formatted: Body Text, Line spacing: Double

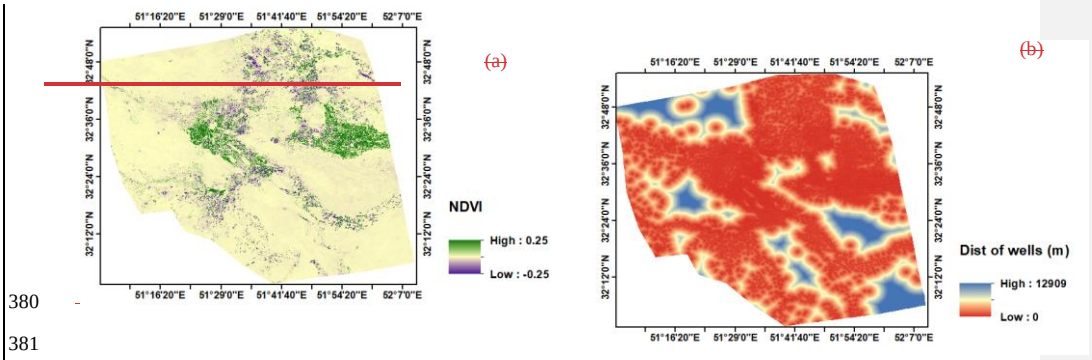

(a) (b)

380

381

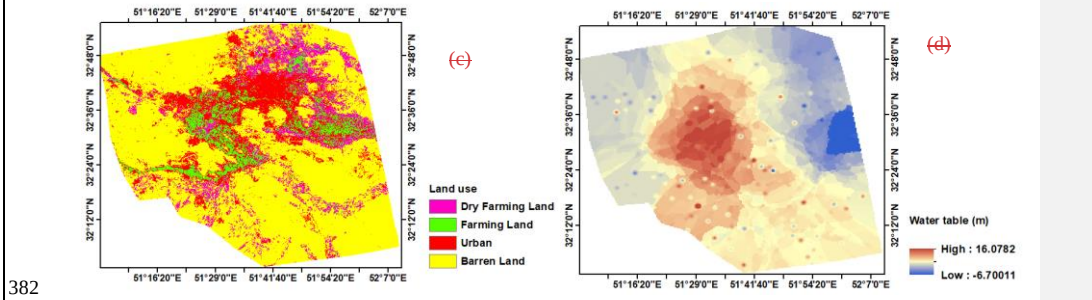

(c) (d)

382

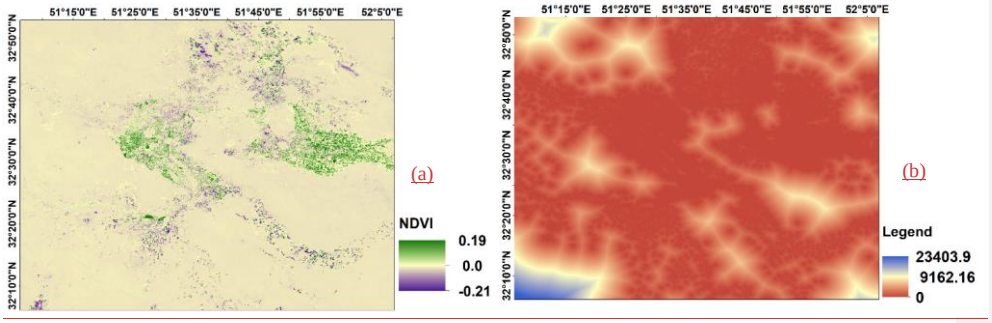

(a) (b)

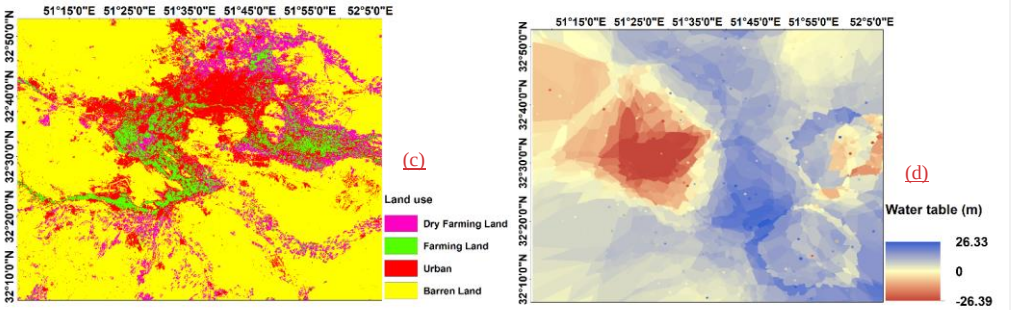

Figure 45: Driving forces of subsidence- (a) NDVI (b) Distance of Wells (c) Land use, (d) Water table map in 20182014 to 2020

4. Result

4.1. Results of CNN

CNN was trained using the calculated driving forces and subsidence at the PSs and the performance of the network by analysing the graphs of the cost function (mean squared error) for the training and validation data, as shown in Figure 56, the MSERMSE values of this model for the training, validation and test data are 5, 93.99, 8.47 and 119 mm, respectively.

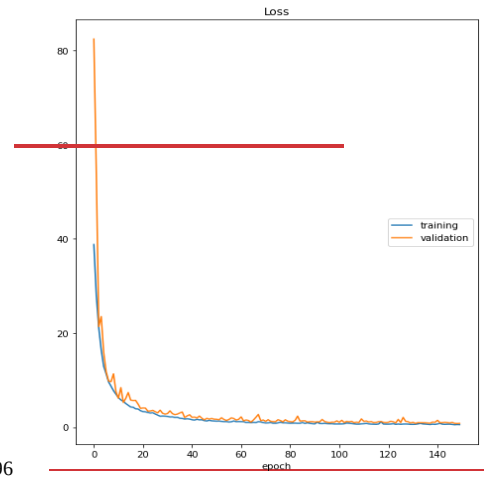

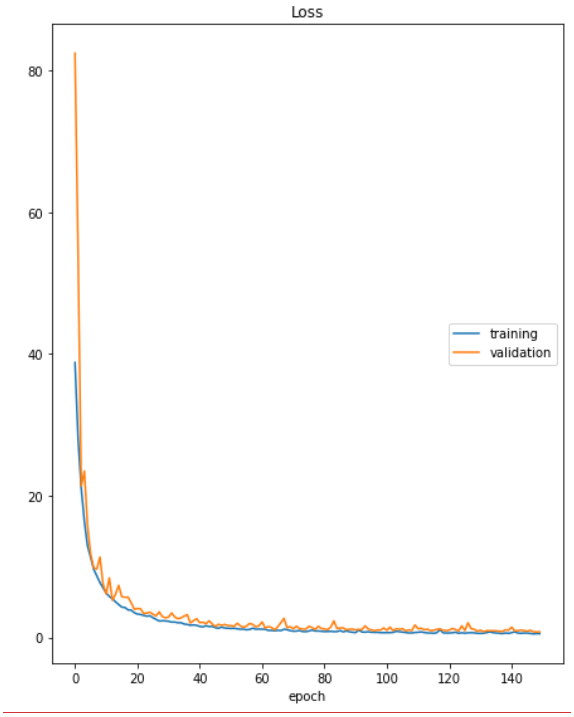

Figure ~~5~~6: Cost function of training and validation data

Formatted: Line spacing: single

4.2. Comparison between CNN and ~~Kriging~~traditional interpolation methods

~~We~~ In our study, we employed ~~two~~four distinct methods to create ~~continuous subsidence surface: interpolation and CNN. To establish~~a continuous subsidence surface: a Convolutional Neural Network (CNN) and three traditional interpolation methods—Kriging, Inverse Distance Weighting (IDW), and Radial Basis Function (RBF). The traditional interpolation methods were utilized to interpolate between Persistent Scatterers (PSs) and calculate the subsidence across all pixels within the study area, based solely on the spatial distribution of the PSs. However, these methods do not account for the subsidence driving forces, and their accuracy can be compromised by irregular distributions of PSs.

In contrast, the CNN approach was trained using subsidence driving forces to predict subsidence and generate a continuous subsidence surface ~~within the study area, we utilized Kriging interpolation.~~ This method ~~only performs interpolation between the PSs and calculates the subsidence of all the pixels~~ is particularly effective in ~~the study area and does not consider the subsidence driving forces. In contrast, a CNN was trained using subsidence-driving forces and used to predict subsidence, producing a continuous subsidence surface with higher reliability. CNN can effectively handle~~handling irregularly distributed data points, making ~~them~~it suitable for scenarios where PSs ~~may not be evenly~~are unevenly distributed across the study area. ~~Kriging relies on the spatial distribution of data points, and irregular distributions can impact its accuracy.~~ By incorporating subsidence driving forces, the CNN can provide a more reliable prediction of subsidence compared to the traditional interpolation methods. To evaluate the accuracy of these methods in predicting subsidence, we used several performance metrics, including the Root Mean Squared Error (RMSE), Mean Absolute Error (MAE) and R-squared (R2), The values of these metrics for each method on the train and test data are given in Table 2. To further validate the superiority of the CNN model, we conducted statistical significance tests. A t-Test was performed to compare the performance metrics, with the results indicating a statistically significant improvement in the CNN model's performance over the traditional interpolation methods (p-value < 0.05). These results indicate a statistically significant improvement in the accuracy of the CNN compared to the traditional interpolation methods.

~~**To assess the accuracy of these methods in predicting subsidence, we calculated MSE for both the methods, MSE of CNN, Kriging is 11 and 37.19 mm, respectively. By comparing these outcomes, we can evaluate the effectiveness of both interpolation and CNN in predicting land subsidence.**~~**Table 2 . Compare between interpolation methods to predict subsidence (Train data)**

Train data	Test data

Formatted: English (United States)
Formatted: English (United States)
Formatted: English (United States)
Formatted: English (United States)
Formatted: English (United States)
Formatted: English (United States)
Formatted: English (United States)
Formatted: English (United States)
Formatted: English (United States)

Method	RMSE (mm)	MAE (mm)	R2 score	RMSE (mm)	MAE (mm)	R2 score
CNN	3.99	2.18	0.99	9.06	3.69	0.98
Kriging	62.78	39.19	-0.09	61.60	37.90	-0.06
IDW	67.32	40.52	-0.25	66.21	39.30	-0.22
RBF	62.67	38.95	-0.08	61.76	37.92	-0.06

Error distribution maps are visual tools that illustrate the spatial distribution of prediction errors across the study area. These maps play a crucial role in evaluating the performance of subsidence prediction models, such as the Convolutional Neural Network (CNN) and traditional interpolation methods (Kriging, IDW, and RBF).

By plotting the differences between the predicted and PSInSAR subsidence values at various locations, error distribution maps help identify patterns or areas where the models perform well or poorly. Clusters of high errors indicate that traditional interpolation methods do not perform well in areas where the range of subsidence values is greater than the average values of the entire study area and in areas with sparse PS distribution. These methods tend to have the highest errors at these points, which are often critical for accurate subsidence assessment. In contrast, the CNN demonstrates more consistent performance due to its training on subsidence driving forces, resulting in lower errors in these high-variance regions.

In our study, the error distribution maps confirmed the findings from the quantitative performance metrics (RMSE, MAE, and R^2 score). The CNN showed a more uniform error distribution, indicating its effectiveness in handling irregular data distributions and incorporating subsidence driving forces. This visual evidence supports the conclusion that the CNN provides a more reliable and accurate subsidence prediction compared to traditional interpolation methods (Fig. 7).

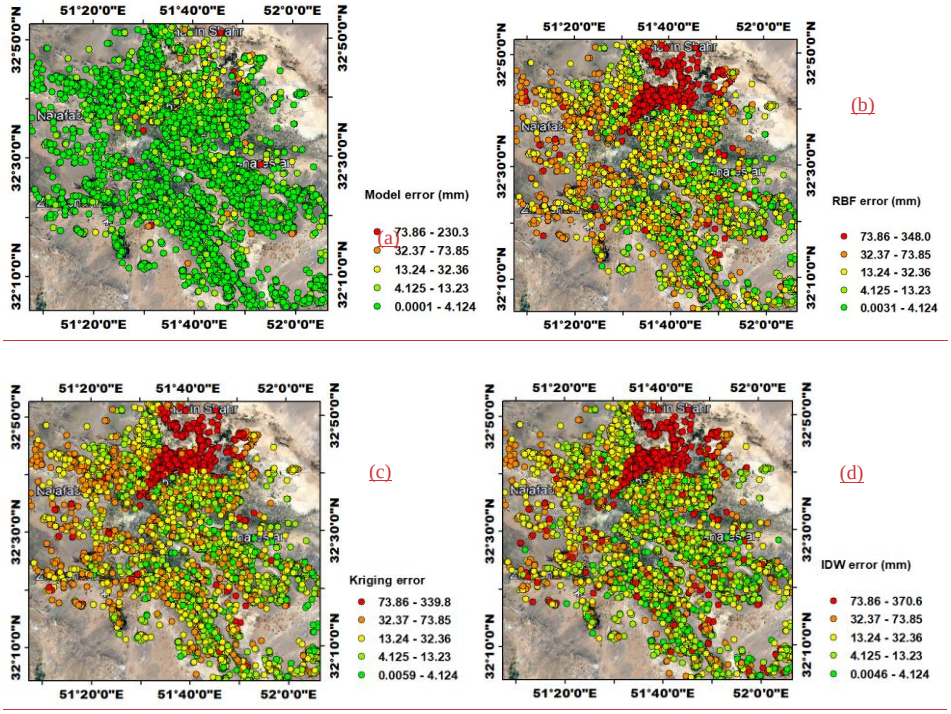

Figure 7: Error distribution map of (a) CNN (b) RBF (c) Kriging (d) IDW

4.3 Subsidence of Study area

In our analysis of land subsidence in the Isfahan region, we processed a total of 73 Sentinel-A images using the PSInSAR method. Through this process, we identified PSs by applying a range amplitude dispersion index threshold of 0.2 and a temporal correlation threshold of 0.8. The maximum velocity for these PSs was observed in the northeast of the study area, specifically near Shahid Beheshti Airport in Isfahan, measuring at -67 mm per year. This significant rate resulted in a cumulative displacement of approximately -33 cm in the period from 2014 to 2020 (Fig. ~~6~~8).

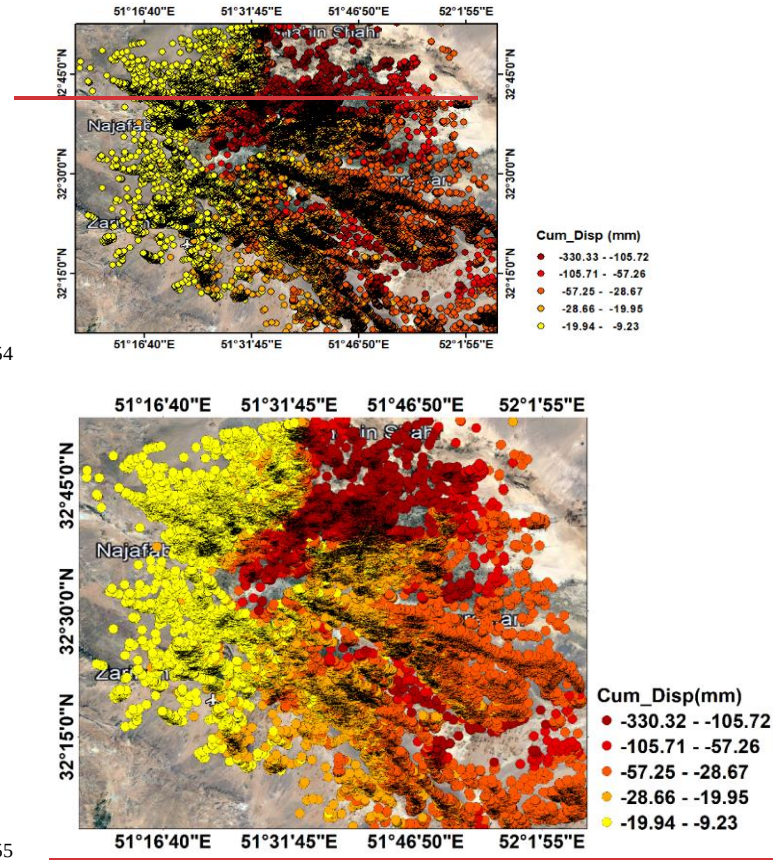

Figure 6~~8~~: Cumulative displacement of PSs in 2014 to 2020

A velocity map was created using Kriging interpolation between PSs. The results showed that the highest velocity, approximately 67 mm per year, was observed in the northeast of the study area (Fig. ~~7~~9).

Formatted: Justify Low, Line spacing: single

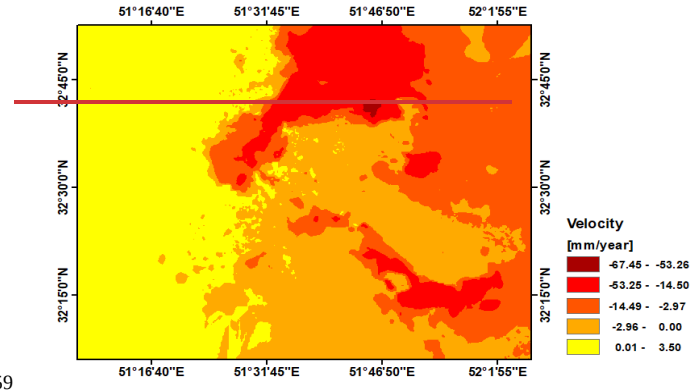

459

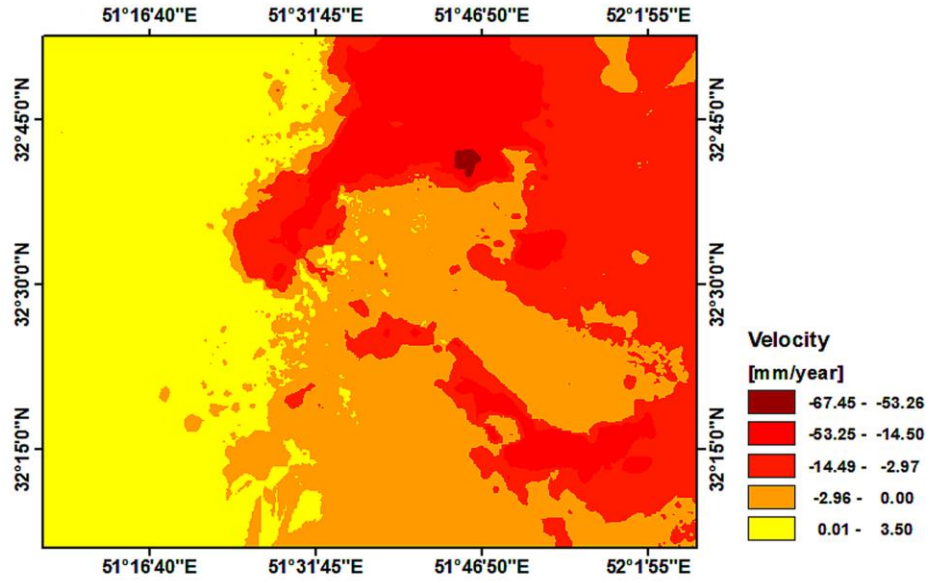

460

461 **Figure ~~7~~9: Velocity map using Kriging**

462 In this research, in order to obtain a continuous subsidence surface of a specific area, two methods, Kriging and CNN,
463 Kriging method is based on mathematics and interpolation between cumulative displacement of PSs. The maximum
464 amount of cumulative displacement obtained by the Kriging method in the studied area is approximately 36 cm (Fig.
465 ~~8~~10).

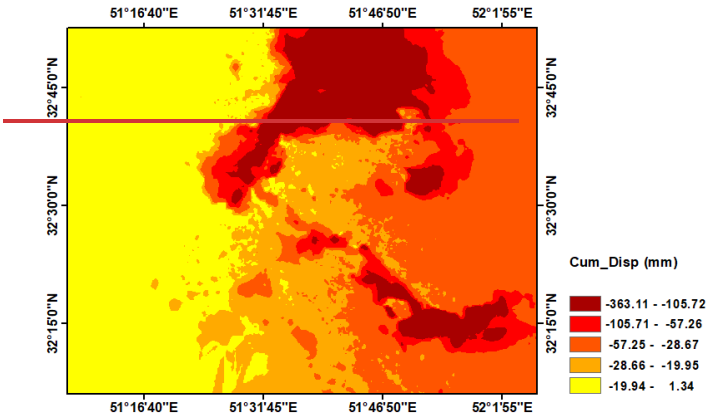

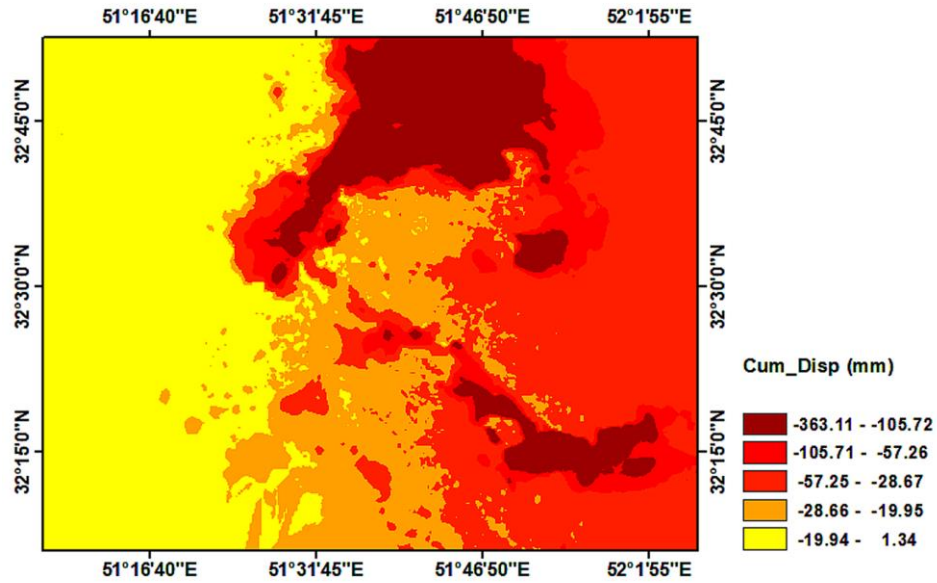

Figure ~~8~~10: Cumulative displacement using Kriging in 2014 to 2020

The CNN method was trained with the cumulative displacement of PSs and the subsidence driving forces in these points, and finally the subsidence of the entire area was predicted with this model. The maximum amount of cumulative displacement obtained by the CNN method in the studied area is approximately 33 cm (Fig. ~~9~~11).

Formatted: Font: 9 pt, Complex Script Font: 9 pt

Formatted: Line spacing: single

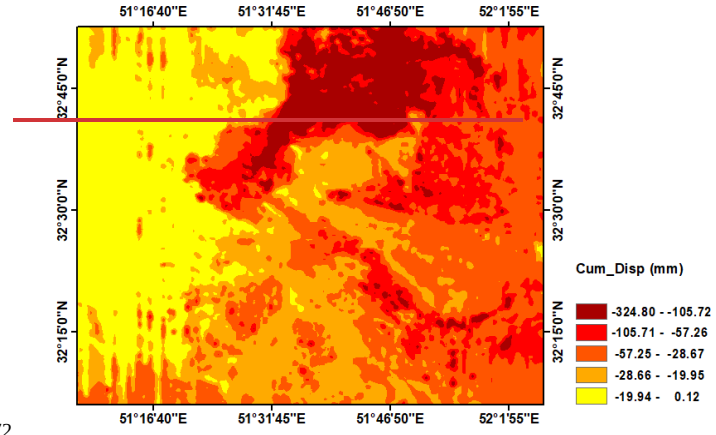

472

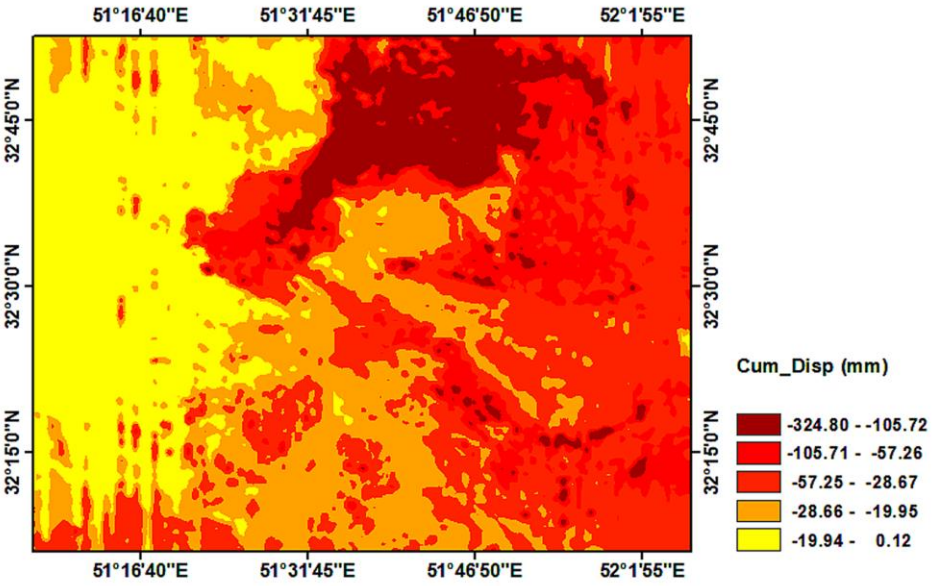

473

474 **Figure 11: Cumulative displacement using CNN in 2014 to 2020**

475

476 Shahid Beheshti Airport in Isfahan is ~~currently facing~~experiencing a ~~concerning situation~~critical rate of land

477 subsidence, with ~~the~~an estimated velocity ~~reaching more than~~exceeding 45 mm ~~each~~per year. This alarming rate of

Formatted: Font: Bold

Formatted: Line spacing: single

deformation has resulted in a significant cumulative displacement of approximately 41 cm ~~in the region from~~between 2014 ~~to~~and 2020. ~~In addition~~Moreover, the CNN-generated subsidence map ~~produced by CNN shows that the~~reveals a slightly higher maximum cumulative displacement ~~in this area has reached~~ of 42 cm~~. Our study also revealed noteworthy~~ in the region, suggesting that deep learning models provide a more comprehensive and accurate representation of land deformation. These findings ~~for Mahyar and Nasr Abad Jarqouye. In these~~highlight the urgency of addressing subsidence-related risks, particularly in critical infrastructure areas~~, the velocity is approximately 5 cm per year, resulting in a maximum cumulative displacement of approximately 33 cm between 2014 and 2020.~~ such as airports, where even slight ground movements can lead to substantial damage. The ~~maximum cumulative displacement using kriging interpolation showed approximately 35 cm. However, the maximum cumulative displacement using~~ CNN ~~showed approximately 32 cm (Fig. 10).~~model's ability to detect and quantify subsidence in regions with sparse data further underscores its potential as a valuable tool for monitoring and mitigating land deformation across various urban and industrial settings (Fig. 12).

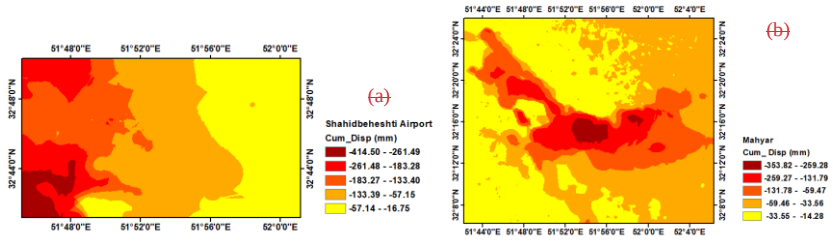

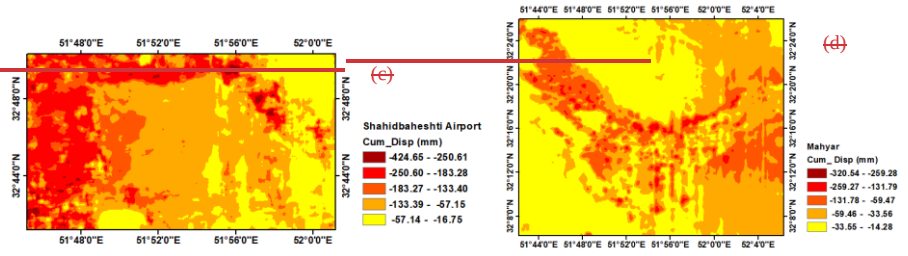

496

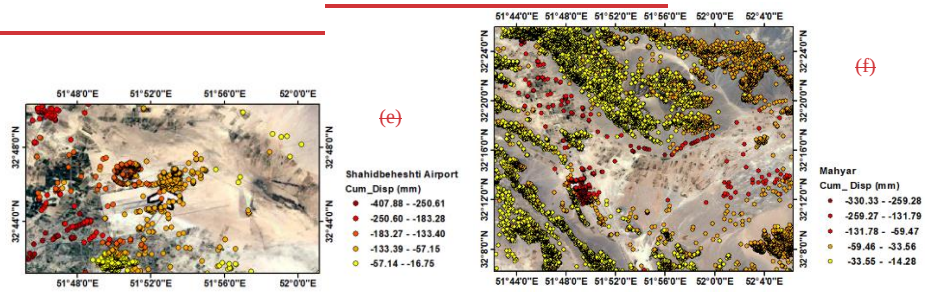

497

498

499

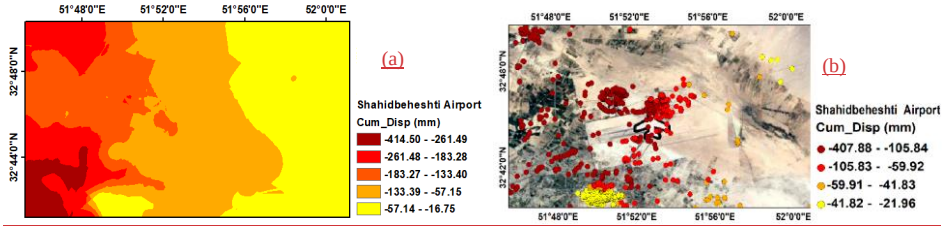

500

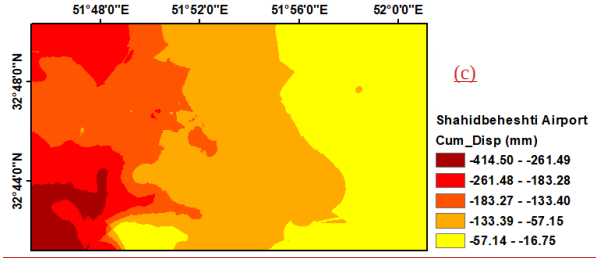

501

Figure ~~12.~~4: Cumulative Displacement of Shahid Beheshti Airport ~~and Mahyar and Nasr Abad Jarqouye~~ in 2014 to 2020: (a~~),~~ ~~(b~~) Continuous surface of cumulative displacement using Kriging interpolation between PSs (~~c), (d~~b) Cumulative displacement of PSs (c) Continuous surface of cumulative displacement ~~(e), (f) Cumulative displacement of PSs~~

~~In~~Our study revealed significant subsidence patterns in the Mahyar and Nasr Abad Jarqouye regions, highlighting the severity of land deformation over the observation period. The analysis indicates an average subsidence velocity of approximately 5 cm per year, leading to a substantial cumulative displacement of around 33 cm between 2014 and 2020. When applying the ~~Naqsh~~ Kriging interpolation method, the estimated maximum cumulative displacement reached approximately 35 cm. In contrast, our deep learning-based CNN model predicted a slightly lower maximum cumulative displacement of around 32 cm (Fig. 13). These findings underscore the variations in prediction accuracy between traditional geostatistical methods and data-driven deep learning approaches. The discrepancy between Kriging and CNN estimates suggests that while Kriging may slightly overestimate extreme displacement values due to its spatial smoothing effect, the CNN model, trained directly on observed deformation patterns, offers a more data-driven approach to subsidence prediction.

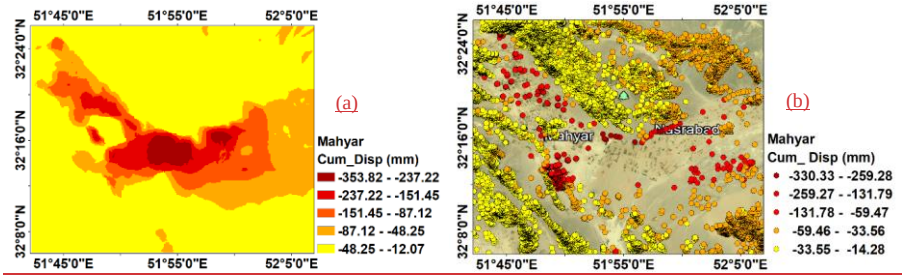

Formatted: Font: Bold

Formatted: English (United States)

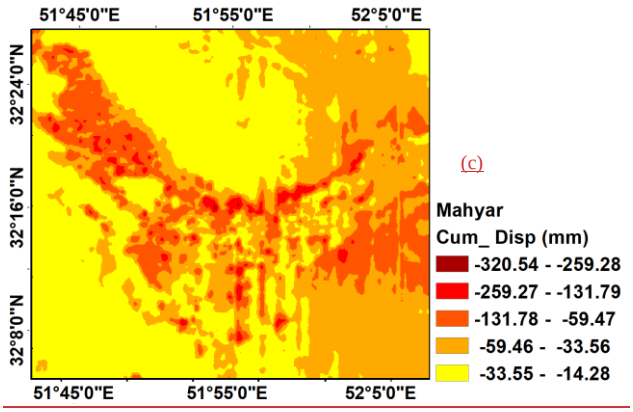

Figure 5: Cumulative Displacement of Mahyar and Nasr Abad Jarqouye in 2014 to 2020: (a) Continuous surface of cumulative displacement using Kriging interpolation between PSs (b) Cumulative displacement of PSs (c) Continuous surface of cumulative displacement

In the Naqsheh Jahan area, the maximum cumulative displacement estimated ~~through~~using the ~~kriging~~Kriging and CNN methods between 2014 and 2020 was approximately 6 cm and 12 cm, respectively. ~~Meanwhile at~~Similarly, in the Si-o-Se Pol area, the Kriging method estimated a maximum cumulative displacement ~~estimated through the kriging and CNN methods between 2014 and 2020 was approximately~~of around 6 cm ~~and~~ , while the CNN predicted a significantly higher value of approximately 19 cm~~, respectively (Fig. 11).~~ . These discrepancies highlight fundamental differences between geostatistical interpolation and deep learning-based predictive modeling. While Kriging interpolation effectively fits observed PSs, it struggles with accurate extrapolation in regions where measurement points are sparse or absent. Conversely, CNN approach identifies significant deformation trends that Kriging fails to detect, emphasizing the potential of deep learning techniques for more reliable and spatially comprehensive subsidence prediction (Fig. 14).

Formatted: English (United States)
Formatted: English (United States)
Formatted: English (United States)
Formatted: English (United States)
Formatted: English (United States)
Formatted: English (United States)
Formatted: English (United States)
Formatted: English (United States)

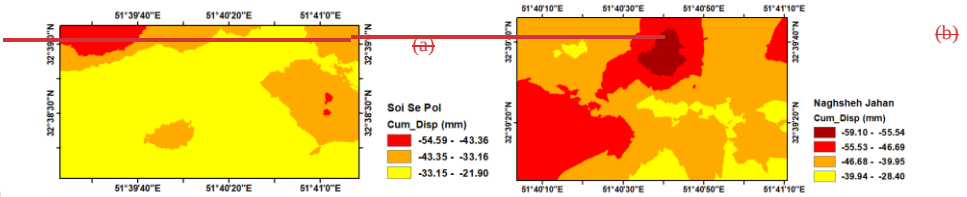
(a)
Soi Se Pol
Cum_Disp (mm)
-54.59 - -43.36
-43.35 - -33.16
-33.15 - -21.90
(b)
Naghsheh Jahan
Cum_Disp (mm)
-59.10 - -55.54
-55.53 - -46.69
-46.68 - -39.95
-39.94 - -28.40

534

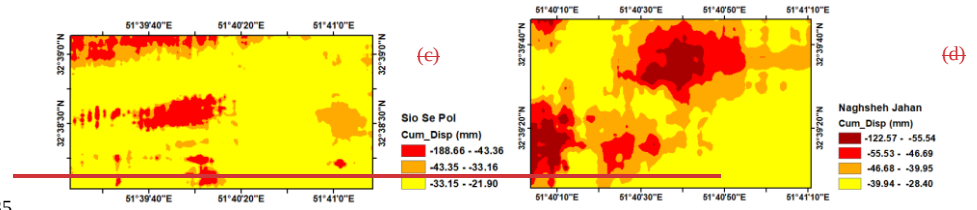
(c)
Sio Se Pol
Cum_Disp (mm)
-188.66 - -43.36
-43.35 - -33.16
-33.15 - -21.90
(d)
Naghsheh Jahan
Cum_Disp (mm)
-122.57 - -55.54
-55.53 - -46.69
-46.68 - -39.95
-39.94 - -28.40

535

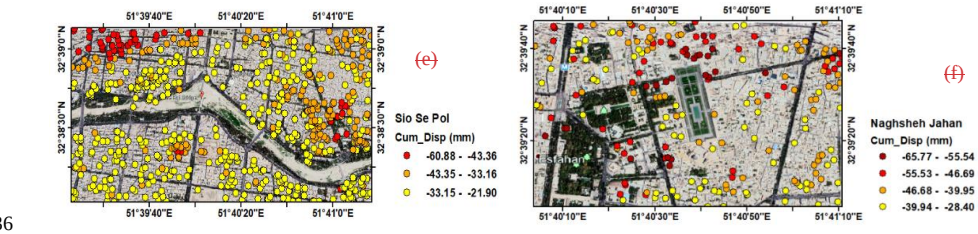
(e)
Sio Se Pol
Cum_Disp (mm)
-60.88 - -43.36
-43.35 - -33.16
-33.15 - -21.90
(f)
Naghsheh Jahan
Cum_Disp (mm)
-65.77 - -55.54
-55.53 - -46.69
-46.68 - -39.95
-39.94 - -28.40

536

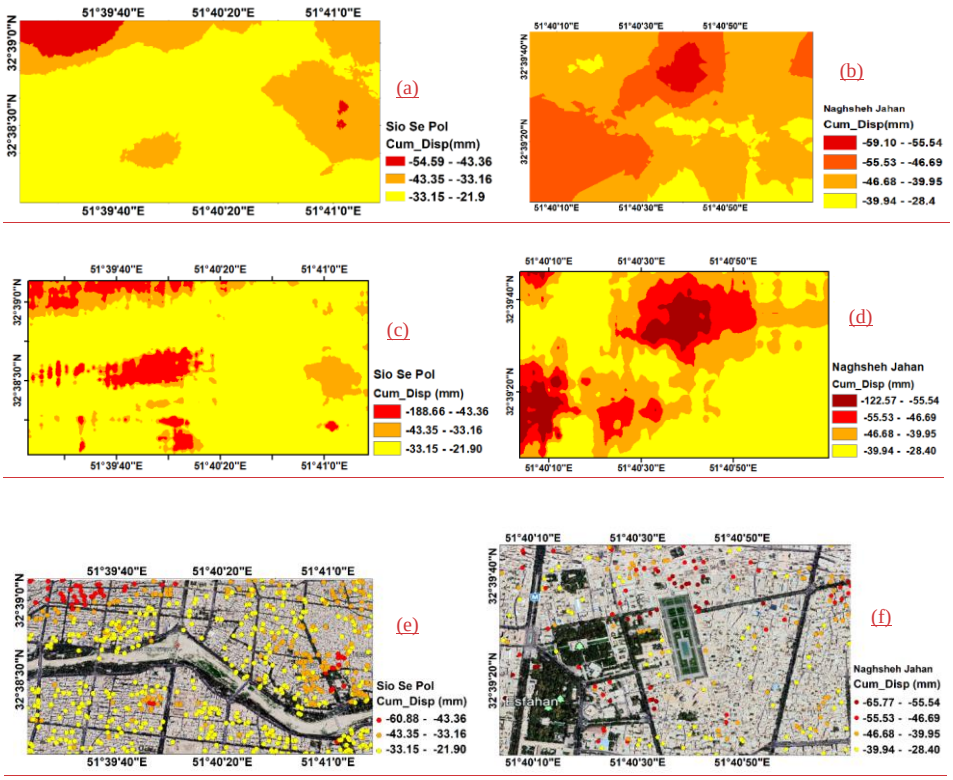

Figure ~~11.~~6: Cumulative Displacement of ~~Naqsh~~ Naghsheh Jahan and Si-o-Se Pol area, 2014 to 2020: (a), (b) Continuous surface of cumulative displacement using Kriging interpolation between PSs (c), (d) Cumulative displacement of PSs (e), (f) Continuous surface of cumulative displacement resulting from CNN ~~(e), (f) Cumulative displacement of PSs~~

Formatted: Caption

The city of Khomeini Shahr is facing a concerning situation where the velocity has been estimated to be more than 45 mm per year. Unfortunately, this has resulted in displacement in residential areas, with the maximum cumulative displacement of PSs reaching 30 cm from 2014 to 2020. According to the map generated using CNN, the maximum cumulative displacement is currently at 31 cm. ~~It has been estimated that the velocity in Falavarjan city is more than 23 mm per year, which is concerning. As a result, there has been a maximum cumulative displacement of 16 cm in the area from 2014 to 2020. According to the CNN-generated map, the maximum cumulative displacement in Falavarjan is 23 cm (Fig. 12).~~A comparative analysis of Kriging interpolation and the CNN model against PSInSAR observations reveals key methodological differences. The Kriging interpolation method, while effective in fitting observed data points, primarily relies on mathematical interpolation and spatial smoothing. This often leads to

inaccuracies in regions with a lower density of PS points, as it lacks the ability to infer displacement patterns beyond the available observations. In contrast, the CNN model estimates settlement values based on learned structural relationships, capturing complex spatial dependencies and underlying deformation mechanisms more effectively. This advantage allows the deep learning model to provide a more continuous and spatially coherent subsidence map, improving predictive accuracy in areas with sparse measurement data (Fig. 15).

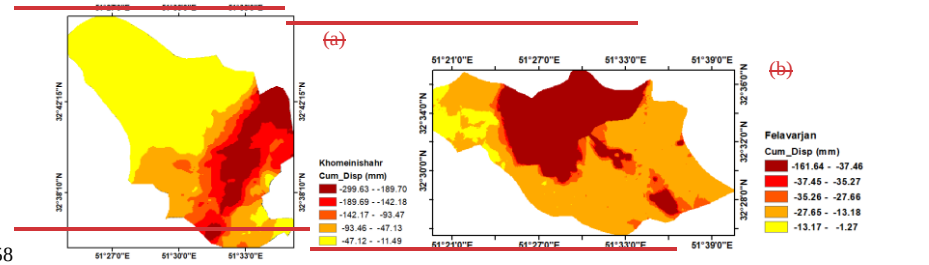

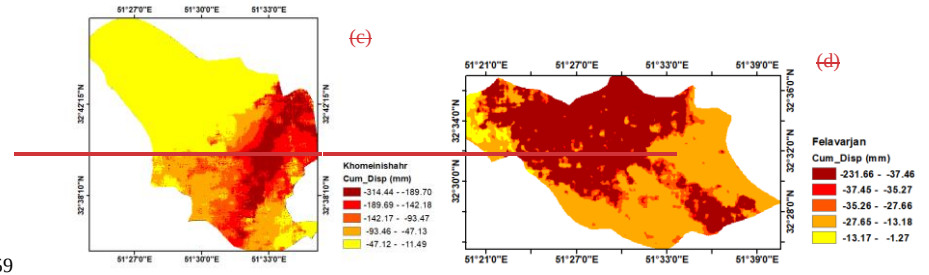

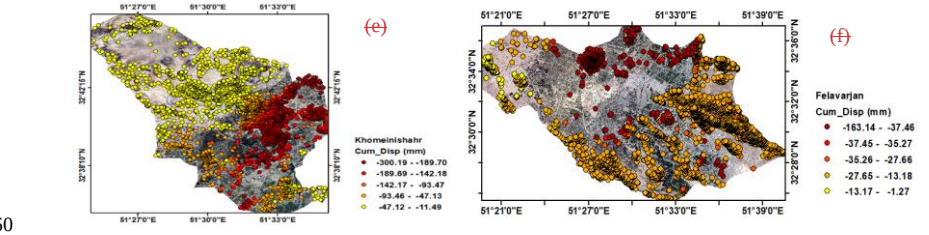

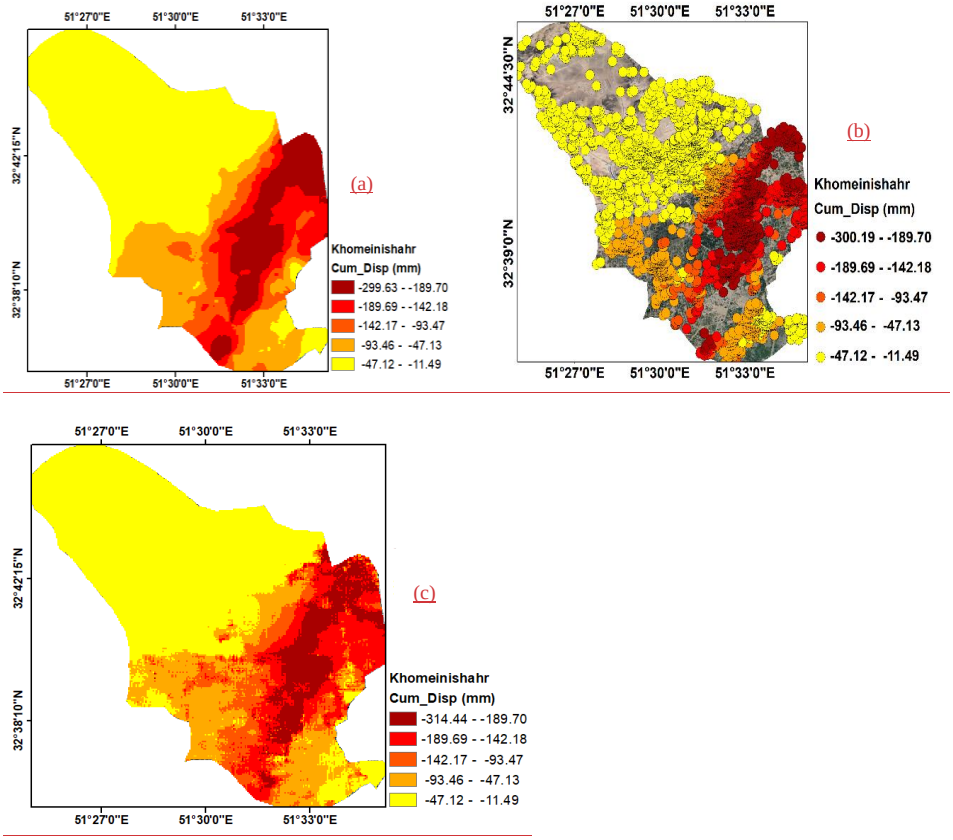

Figure ~~12.~~7: Cumulative Displacement of Khomeini Shahr ~~and Falavarjan~~, 2014 to 2020: (a~~), (b~~) Continuous surface of cumulative displacement using Kriging interpolation between PSs (~~c), (d~~b) Cumulative displacement of PSs (c) Continuous surface of cumulative displacement resulting from CNN ~~(e), (f) Cumulative displacement of PSs~~

Formatted: Line spacing: single

In Falavarjan city, the estimated subsidence velocity exceeds 23 mm per year, highlighting a concerning rate of land deformation. Over the period from 2014 to 2020, this has resulted in a maximum cumulative displacement of approximately 16 cm based on conventional geostatistical estimates. However, the CNN-generated subsidence map indicates a significantly higher maximum cumulative displacement of around 23 cm. The discrepancy between PSInSAR estimates and CNN predictions highlights fundamental differences in their modeling approaches. While conventional methods rely on spatial interpolation and statistical assumptions, CNNs leverage spatial dependencies and structural patterns learned from observed data, allowing for more accurate and continuous subsidence mapping.

This suggests that deep learning-based approaches may provide a more reliable representation of ground deformation, particularly in regions with a sparse distribution or absence of PSs (Fig. 16).

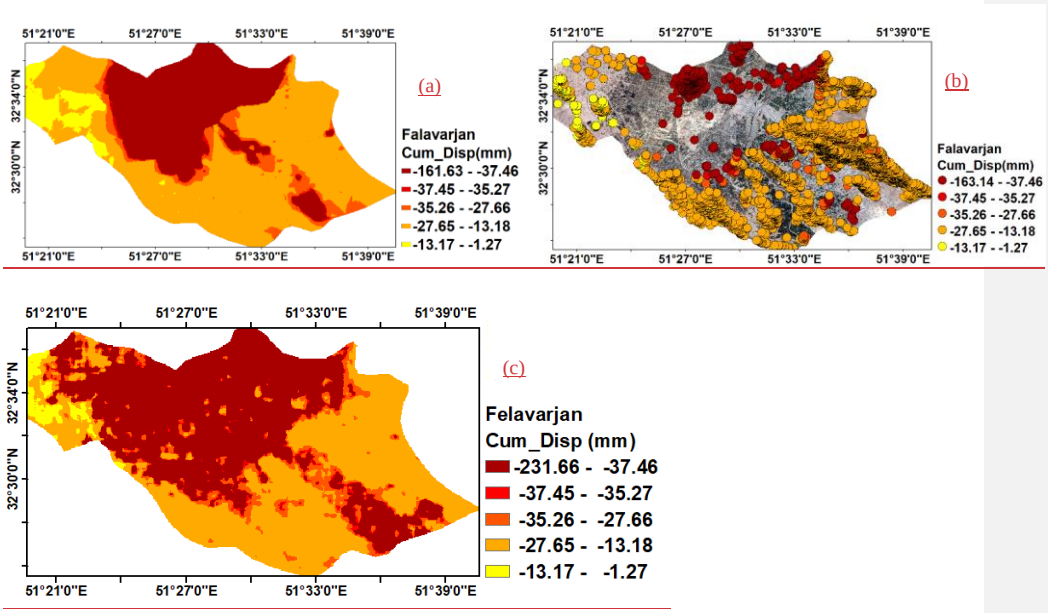

Figure 8: Cumulative Displacement of Falavarjan, 2014 to 2020: (a) Continuous surface of cumulative displacement using Kriging interpolation between PSs (b) Cumulative displacement of PSs (c) Continuous surface of cumulative displacement resulting from CNN

Data Availability

~~The SAR Sentinel-1A dataset used in this study is freely available for access on the web at https://dataspace.copernicus.eu~~

The data used in this study consists of subsidence measurements obtained from Sentinel-1A and Landsat 8 images over the period of 2014-2020. The subsidence was calculated using the Sarproz and driving forces of subsidence was calculated using the ENVI software tools. Sentinel-1A Data: The Sentinel-1A images were used to Calculation of subsidence through PSInSAR in Sarproz (Version [pcodes_2019-10-02]). Landsat 8 Data: The Landsat 8 images were used to calculate Land use and NDVI using ENVI (Version [5.3]). Digital Elevation Model: DEM was used to calculate TWI, SPI, Aspect, Slope, Altitude using ArcGIS (Version [10.7.1]

5. Conclusion

~~The PSInSAR method has proven to be a dependable technique for investigating gradual land deformation, particularly subsidence. However, it yields discrete results limited to PSs only, making it less suitable for areas with vegetation. In such scenarios, Kriging interpolation between PSs is commonly used to create a continuous subsidence surface. Nevertheless, this approach has its limitations due to the complex nature of subsidence influenced by various factors. In our study, we tackled this challenge by generating a continuous subsidence surface for the entire study area using a CNN. We factored in the driving forces of subsidence in this process. We evaluated the accuracy of both Kriging interpolation and CNN methods by calculating the mean square error on the test data. The results revealed that the study area experienced more than 38 cm of subsidence between 2014 and 2020. Notably, the velocity was estimated to be over 45 mm per year at Shahid Beheshti airport, exceeding 54 mm per year in the Mahyar Plain, and around 6 mm per year in Naqsh-Jahan and Sio-Se-Pol Bridges. The mean square error values for the training, validation, and test data using the CNN were determined to be 5 mm, 9 mm, and 11 mm, respectively. These results indicated a significant improvement of 70% in the prediction of subsidence with intelligent interpolation CNN compared to the kriging interpolation method. This CNN-based method offers a robust and accurate interpolation approach, even when dealing with sparse and irregularly distributed data.~~

This study presents an innovative deep learning framework utilizing a Convolutional Neural Network (CNN) to generate a continuous subsidence surface across the study area. Unlike traditional methods that rely on discrete geodetic measurements, the proposed approach integrates multiple key driving factors—including NDVI, distance from wells, land use, water table depth, altitude, slope, SPI, TWI, and aspect—providing a more comprehensive and data-driven understanding of subsidence dynamics. The CNN model effectively addresses the limitations of PSInSAR, which, despite its reliability in detecting gradual land deformation, is restricted to persistent scatterers (PSs) and performs poorly in vegetated or low-coherence areas. By leveraging deep learning, the proposed model enables subsidence estimation even in regions where PSInSAR measurements are unavailable, addressing a critical gap in geospatial monitoring.

The superiority of the CNN-based approach was demonstrated through a comparative analysis against conventional interpolation techniques, including Kriging, IDW, and RBF. The CNN model achieved significantly lower RMSE values (3.99 mm, 8.47 mm, and 9 mm for the training, validation, and test datasets, respectively) and an R^2 score of 0.98, whereas traditional methods exhibited considerably higher RMSE values (Kriging: 61.60 mm, IDW: 66.21 mm,

RBF: 61.76 mm) and negative R^2 scores, highlighting their limitations in subsidence prediction. The study also identified severe land subsidence in key areas, with rates exceeding 45 mm per year at Shahid Beheshti Airport and over 54 mm per year in the Mahyar Plain. The CNN model demonstrated an 85% improvement in prediction accuracy over traditional methods, underscoring its robustness and effectiveness, particularly in areas with sparse and irregularly distributed data.

Despite these advancements, some challenges remain. The model's performance is influenced by the availability and quality of input data, and its computational demands necessitate high-performance GPUs for efficient training. Additionally, regional variations in subsidence mechanisms may require model adaptations to ensure accuracy across diverse landscapes. Future research should focus on enhancing the model's generalizability across different geographical regions, developing real-time monitoring capabilities for early warning systems, and integrating additional datasets—such as climate variables and bedrock depth—to further refine predictive accuracy. Furthermore, exploring hybrid deep learning architectures, such as CNN-LSTM models, may enhance computational efficiency and improve temporal prediction capabilities. Addressing these aspects will further establish deep learning-based subsidence modeling as a scalable and effective tool for geospatial analysis, environmental monitoring, and urban planning.

Code and data availability

~~The code for the CNN model and related data, as described in the paper, can be accessed via the Zenodo archive using the following link: https://zenodo.org/records/10956394 (Azarm,2024)~~

The Excel file in the Zenodo repository contains 62,000 data points corresponding to permanent scatterers obtained from the PSInSAR method. The nine satellite images used as inputs for the model, which include NDVI, Landuse, etc., were calculated using Landsat 8 and DEM images from the area. These images are also available in the Zenodo repository. Additionally, the Python code for the CNN model used in this paper are accessible through the Zenodo archive at the following link: https://zenodo.org/records/12721120 (Azarm, 2024).

Author contribution

Azarm contributed to the writing of the manuscript and conducted the analytic calculations and numerical simulations with the support and supervision of Mehrabi and Nadi. All authors actively participated in discussing the results, providing comments on the manuscript, and revising the final version.

Formatted: Font: Times New Roman

Formatted: Justified, Line spacing: Double, Pattern: Clear

Formatted: English (United Kingdom)

Competing interests

The contact author has declared that none of the authors has any competing interests.

Acknowledgment

The authors gratefully acknowledge the European Space Agency for providing the Sentinel-1 datasets of the Copernicus mission, which were indispensable for this study. They also extend their sincere appreciation to the Isfahan Regional Water Organization for providing the piezometer data. The data were processed using SARPROZ (Copyright (c) 2009-2015 Daniele Perissin) and visualized in Matlab®, with the support of Google Maps and Google Earth. Additionally, the authors would like to express their gratitude to the US Geological Survey for making the SRTM 1 Arc-Second Global DEM data available, which played a crucial role in the data processing and analysis presented in this paper.

References

Sun, M., Du, Y., Liu, Q., Feng, G., Peng, X. and Liao, C.: Understanding the Spatial-Temporal Characteristics of Land Subsidence in Shenzhen under Rapid Urbanization Based on MT-InSAR. IEEE J SEL TOP APPL. ~~10.1109/JSTARS.2023.3264652,~~10.1109/JSTARS.2023.3264652, 2023.

Fialko, Y., Sandwell, D., Simons, M. and Rosen, P.: Three-dimensional deformation caused by the Bam, Iran, earthquake and the origin of shallow slip deficit. CAH REV THE. 435, 295-299, 10.1038/nature03425, 2005.

Hu, J., Li, Z., Ding, X., Zhu, J., Zhang, L. and Sun, Q.: 3D coseismic displacement of 2010 Darfield, New Zealand earthquake estimated from multi-aperture InSAR and D-InSAR measurements. J GEODESY. 86, 1029-1041, https://doi.org/10.1007/s00190-012-0563-6, 2012.

Chang, C.-P., Yen, J.-Y., Hooper, A., Chou, F.-M., Chen, Y.-A., Hou, C.-S., Hung, W.-C. and Lin, M.-S.: Monitoring of Surface Deformation in Northern Taiwan Using DInSAR and PSInSAR Techniques. TAO. 21, https://doi.org/10.3319/TAO.2009.11.20.01(TH), 2010.

Tamburini, A., Bianchi, M., Giannico, C. and Novali, F.: Retrieving surface deformation by PSInSAR™ technology: A powerful tool in reservoir monitoring. INT J GREENH GAS CON. 4, 928-937, https://doi.org/10.1016/j.ijggc.2009.12.009, 2010.

Tomás, R., Herrera, G., Cooksley, G. and Mulas, J.: Persistent Scatterer Interferometry subsidence data exploitation using spatial tools: The Vega Media of the Segura River Basin case study. J HYDROL. ~~400, 411-428, https://doi.org/10.1016/j.jhydrol.2011.01.057,~~400, 411-428, 2011.

Rucci, A., Ferretti, A., Guarnieri, A. M. and Rocca, F.: Sentinel 1 SAR interferometry applications: The outlook for sub millimeter measurements. REMOTE SENS ENVIRON. 120, 156-163, https://doi.org/10.1016/j.rse.2011.09.030, 2012.

Formatted: Left

673 Amighpey, M. and Arabi, S.: Studying land subsidence in Yazd province, Iran, by integration of InSAR and
674 levelling measurements. Remote Sens Appl. 4, 1-8, https://doi.org/10.1016/j.rsase.2016.04.001,4, 1-8, 2016.

675 Biswas, K., Chakravarty, D., Mitra, P. and Misra, A.: Spatial Correlation Based Psinsar Technique to Estimate
676 Ground Deformation in las Vegas Region, Us. 2251-2254, https://doi.org/10.1109/IGARSS.2018.8518123, 2018.

677 Gonnuru, P. and Kumar, S.: PsInSAR based land subsidence estimation of Burgan oil field using TerraSAR-X data.
678 Remote Sens Appl. 9, 17-25, https://doi.org/10.1016/j.rsase.2017.11.003, 2018.

679 Khorrami, M., Alizadeh, B., Ghasemi Tousi, E., Shakerian, M., Maghsoudi, Y. and Rahgozar, P.: How groundwater
680 level fluctuations and geotechnical properties lead to asymmetric subsidence: A PSInSAR analysis of land
681 deformation over a transit corridor in the Los Angeles metropolitan area. REMOTE SENS-BASEL. 11, 377,
682 https://doi.org/10.3390/rs11040377, 2019.

683 Gao, M., Gong, H., Li, X., Chen, B., Zhou, C., Shi, M., Guo, L., Chen, Z., Ni, Z. and Duan, G.: Land subsidence
684 and ground fissures in Beijing capital international airport (bcia): Evidence from quasi-ps insar analysis. REMOTE
685 SENS-BASEL. 11, 1466, https://doi.org/10.3390/rs11121466, 2019.

686 Naghibi, S. A., Khodaei, B. and Hashemi, H.: An integrated InSAR-machine learning approach for ground
687 deformation rate modeling in arid areas. J HYDROL. 608, 127627,
688 https://doi.org/10.1016/j.jhydrol.2022.127627,608, 127627, 2022.

689 Mehrabi, H. and Voosoghi, B.: On estimating the curvature attributes and strain invariants of deformed surface
690 through radial basis functions. COMPUT APPL MATH. 37, 978-995, https://doi.org/10.1007/s40314-016-0380-2,
691 2018.

692 Mehrabi, H. and Voosoghi, B.: Recursive moving least squares. ENG ANAL BOUND ELEM. 58, 119-128,
693 https://doi.org/10.1016/j.enganabound.2015.04.001, 2015.

694 Nie, L., Wang, H., Xu, Y. and Li, Z.: A new prediction model for mining subsidence deformation: the arc tangent
695 function model. NAT HAZARDS. 75, 2185-2198, https://doi.org/10.1007/s11069-014-1421-z, 2015.

696 Zhu, Z.-y., Ling, X.-z., Chen, S.-j., Zhang, F., Wang, L.-n., Wang, Z.-y. and Zou, Z.-y.: Experimental investigation
697 on the train-induced subsidence prediction model of Beiluhe permafrost subgrade along the Qinghai–Tibet railway
698 in China. COLD REG SCI TECHNOL. 62, 67-75, https://doi.org/10.1016/j.coldregions.2010.02.010, 2010.

699 Azarakhsh, Z., Azadbakht, M. and Matkan, A.: Estimation, modeling, and prediction of land subsidence using
700 Sentinel-1 time series in Tehran-Shahriar plain: A machine learning-based investigation. Remote Sens Appl. 25,
701 100691, https://doi.org/10.1016/j.rsase.2021.100691,25, 100691, 2022.

702 Ku, C. Y. and Liu, C. Y.: Modeling of land subsidence using GIS-based artificial neural network in Yunlin County,
703 Taiwan. Sci Rep. 13, 4090, https://doi.org/10.1038/s41598-023-31390-5, 2023.

704 Lee, S., Kang, J. and Kim, J.: Prediction Modeling of Ground Subsidence Risk Based on Machine Learning Using
705 the Attribute Information of Underground Utilities in Urban Areas in Korea. Appl. Sci. 13, 5566,
706 https://doi.org/10.3390/app13095566, 2023.

707 Sadeghi, H., Darzi, A. G., Voosoghi, B., Garakani, A. A., Ghorbani, Z. and Mojtahedi, S. F. F.: Assessing the
708 vulnerability of Iran to subsidence hazard using a hierarchical FUCOM-GIS framework. Remote Sens Appl. 31,
709 100989, https://doi.org/10.1016/j.rsase.2023.100989, 2023.

710 Wang, H., Jia, C., Ding, P., Feng, K., Yang, X. and Zhu, X.: Analysis and prediction of regional land subsidence
711 with InSAR technology and machine learning algorithm. KSCE J CIV ENG. 27, 782-793,
712 https://doi.org/10.1007/s10040-020-02211-0, 2023.

Formatted: Hyperlink, No underline

Field Code Changed

Zhou, Q., Hu, Q., Ai, M., Xiong, C. and Jin, H.: An improved GM (1, 3) model combining terrain factors and neural network error correction for urban land subsidence prediction. Geomat Nat Hazards Risk. 11, 212-229, https://doi.org/10.1080/19475705.2020.1716860, 2020.

Deng, Z., Ke, Y., Gong, H., Li, X. and Li, Z.: Land subsidence prediction in Beijing based on PS-InSAR technique and improved Grey-Markov model. GISCI REMOTE SENS. 54, 797-818, https://doi.org/10.1080/15481603.2017.1331511, 2017.

Fan, H., Cheng, D., Deng, K., Chen, B. and Zhu, C.: Subsidence monitoring using D-InSAR and probability integral prediction modelling in deep mining areas. SURV REV. 47, 438-445, https://doi.org/10.1179/1752270614Y.0000000153, 2015.

Mohammady, M., Pourghasemi, H. R. and Amiri, M.: Land subsidence susceptibility assessment using random forest machine learning algorithm. ENVIRON EARTH SCI. 78, 1-12, https://doi.org/10.1007/s12665-019-8518-3, 2019.

Ghorbanzadeh, O., Blaschke, T., Aryal, J. and Gholaminia, K.: A new GIS-based technique using an adaptive neuro-fuzzy inference system for land subsidence susceptibility mapping. J SPAT SCI. 65, 401-418, https://doi.org/10.1080/14498596.2018.1505564, 2020.

Kumar, S., Kumar, D., Donta, P. K. and Amgoth, T.: Land subsidence prediction using recurrent neural networks. Stochastic Environmental Research and Risk Assessment. 36, 373-388, https://doi.org/10.1007/s00477-021-02138-2 2022.

Radman, A., Akhoondzadeh, M. and Hosseiny, B.: Integrating InSAR and deep-learning for modeling and predicting subsidence over the adjacent area of Lake Urmia, Iran. GISCI REMOTE SENS. 58, 1413-1433, https://doi.org/10.1080/15481603.2021.1991689, 2021.

Ma, P., Zhang, F. and Lin, H.: Prediction of InSAR time-series deformation using deep convolutional neural networks. Remote sensing letters. 11, 137-145, https://doi.org/10.1080/2150704X.2019.1692390, 2020.

Ferretti, A., Prati, C. and Rocca, F.: Permanent scatterers in SAR interferometry. IEEE T GEOSCI REMOTE. 39, 8-20, https://doi.org/10.1109/36.898661, 2001.

Wasowski, J. and Bovenga, F.: Investigating landslides and unstable slopes with satellite Multi Temporal Interferometry: Current issues and future perspectives. ENG GEOL. 174, 103-138, https://doi.org/10.1016/j.enggeo.2014.03.003, 2014.

Crosetto, M., Monserrat, O., Cuevas-González, M., Devanthéry, N. and Crippa, B.: Persistent scatterer interferometry: A review. ISPRS J PHOTOGRAMM. 115, 78-89, https://doi.org/10.1016/j.isprsjprs.2015.10.011, 2016.

Ferretti, A., Prati, C. and Rocca, F.: Nonlinear subsidence rate estimation using permanent scatterers in differential SAR interferometry. IEEE T GEOSCI REMOTE. 38, 2202-2212, https://doi.org/10.1109/36.868878, 2000.

Luo, Q., Perissin, D., Lin, H., Zhang, Y. and Wang, W.: Subsidence monitoring of Tianjin suburbs by TerraSAR-X persistent scatterers interferometry. IEEE J SEL TOP APPL. 7, 1642-1650, https://doi.org/10.1109/JSTARS.2013.2271501, 2013.

Peltier, A., Bianchi, M., Kaminski, E., Komorowski, J. C., Rucci, A. and Staudacher, T.: PSInSAR as a new tool to monitor pre-eruptive volcano ground deformation: Validation using GPS measurements on Piton de la Fournaise. GEOPHYS RES LETT. 37, https://doi.org/10.1029/2010GL043846, 2010.

Din, A., Reba, M., Omar, K. M., Razli, M. R. b. M. and Rusli, N.: Land subsidence monitoring using persistent scatterer InSAR (PSInSAR) in Kelantan catchment. 2015.

Formatted: Left

754 Oštir, K. and Komac, M.: PSInSAR and DInSAR methodology comparison and their applicability in the field of
755 surface deformations—a case of NW Slovenia. Geologija. 50, 77-96, https://doi.org/10.5474/geologija.2007.007,
756 2007.

757 Conway, B. D.: Land subsidence and earth fissures in south-central and southern Arizona, USA. HYDROGEOL J.
758 24, 649, https://doi.org/10.1007/s10040-015-1329-z, 2016.

759 Li, D., Liao, M. and Wang, Y.: Progress of permanent scatterer interferometry. Geomat. Inf. Sci. Wuhan Univ. 29,
760 10-24, 2004.

761 Lee, J. G., Jun, S., Cho, Y. W., Lee, H., Kim, G. B., Seo, J. B. and Kim, N.: Deep Learning in Medical Imaging:
762 General Overview. KOREAN J RADIOL. 18, 570-584, https://doi.org/10.3348/kjr.2017.18.4.570, 2017.

763 LeCun, Y. and Bengio, Y.: Convolutional networks for images, speech, and time series. The handbook of brain
764 theory and neural networks. 3361, 1995, 1995.

765 Nair, V. and Hinton, G. E.: Rectified linear units improve restricted boltzmann machines. 807-814, 2010.

766 Van Do, Q., Hoang, H. T., Van Vu, N., De Jesus, D. A., Brea, L. S., Nguyen, H. X., Nguyen, A. T. L., Le, T. N.,
767 Dinh, D. T. M. and Nguyen, M. T. B.: Segmentation of hard exudate lesions in color fundus image using two-stage
768 CNN-based methods. Expert Systems with Applications. ~~241, 122742,~~
769 ~~https://doi.org/10.1016/j.eswa.2023.122742,~~241, 122742, 2024.

770 Christ, P. F., Elshaer, M. E. A., Ettlinger, F., Tatavarty, S., Bickel, M., Bilic, P., Rempfler, M., Armbruster, M.,
771 Hofmann, F. and D'Anastasi, M.: Automatic liver and lesion segmentation in CT using cascaded fully convolutional
772 neural networks and 3D conditional random fields. 415-423, 2016.

773 Lakhani, P. and Sundaram, B.: Deep learning at chest radiography: automated classification of pulmonary
774 tuberculosis by using convolutional neural networks. RADIOLOGY. 284, 574-582,
775 https://doi.org/10.1148/radiol.2017162326, 2017.

776 Elboushaki, A., Hannane, R., Afdel, K. and Koutti, L.: MultiD-CNN: A multi-dimensional feature learning approach
777 based on deep convolutional networks for gesture recognition in RGB-D image sequences. Expert Systems with
778 Applications. ~~139, 112829, https://doi.org/10.1016/j.eswa.2019.112829,~~139, 112829, 2020.

779 Kim, K. H., Choi, S. H. and Park, S. H.: Improving Arterial Spin Labeling by Using Deep Learning. RADIOLOGY.
780 287, 658-666, https://doi.org/10.1148/radiol.2017171154, 2018.

781 Liu, F., Jang, H., Kijowski, R., Bradshaw, T. and McMillan, A. B.: Deep learning MR imaging–based attenuation
782 correction for PET/MR imaging. RADIOLOGY. 286, 676-684, https://doi.org/10.1148/radiol.2017170700, 2018.

783 Chen, M. C., Ball, R. L., Yang, L., Moradzadeh, N., Chapman, B. E., Larson, D. B., Langlotz, C. P., Amrhein, T. J.
784 and Lungren, M. P.: Deep Learning to Classify Radiology Free-Text Reports. RADIOLOGY. 286, 845-852,
785 https://doi.org/10.1148/radiol.2017171115, 2018.

786 Yang, C.-s., Zhang, Q., Zhao, C.-y., Wang, Q.-l. and Ji, L.-y.: Monitoring land subsidence and fault deformation
787 using the small baseline subset InSAR technique: A case study in the Datong Basin, China. J GEODYN. 75, 34-40,
788 https://doi.org/10.1016/j.jog.2014.02.002, 2014.

789 Abdollahi, S., Pourghasemi, H. R., Ghanbarian, G. A. and Safaeian, R.: Prioritization of effective factors in the
790 occurrence of land subsidence and its susceptibility mapping using an SVM model and their different kernel
791 functions. B ENG GEOL ENVIRON. 78, 4017-4034, https://doi.org/10.1007/s10064-018-1403-6, 2019.

792 Andaryani, S., Nourani, V., Trolle, D., Dehghani, M. and Asl, A. M.: Assessment of land use and climate change
793 effects on land subsidence using a hydrological model and radar technique. J HYDROL. ~~578, 124070,~~
794 ~~https://doi.org/10.1016/j.jhydrol.2019.124070,~~578, 124070, 2019.

Formatted: Default Paragraph Font, Font: Times New Roman, Font color: Auto

Zang, M., Peng, J. and Qi, S.: Earth fissures developed within collapsible loess area caused by groundwater uplift in Weihe watershed, northwestern China. J ASIAN EARTH SCI. 173, 364-373, https://doi.org/10.1016/j.jseaes.2019.01.034, 2019.

Shi, L., Gong, H., Chen, B. and Zhou, C.: Land subsidence prediction induced by multiple factors using machine learning method. REMOTE SENS-BASEL. 12, 4044, https://doi.org/10.3390/rs12244044, 2020.

Zhao, Y., Wang, C., Yang, J. and Bi, J.: Coupling model of groundwater and land subsidence and simulation of emergency water supply in Ningbo urban Area, China. J HYDROL. ~~594, 125956,~~ ~~https://doi.org/10.1016/j.jhydrol.2021.125956,~~594, 125956, 2021.

Pradhan, B., Abokharima, M. H., Jebur, M. N. and Tehrany, M. S.: Land subsidence susceptibility mapping at Kinta Valley (Malaysia) using the evidential belief function model in GIS. NAT HAZARDS. 73, 1019-1042, https://doi.org/10.1007/s11069-014-1128-1

2014.

Qin, C.-Z., Zhu, A.-X., Pei, T., Li, B.-L., Scholten, T., Behrens, T. and Zhou, C.-H.: An approach to computing topographic wetness index based on maximum downslope gradient. PRECIS AGRIC. 12, 32-43, https://doi.org/10.1007/s11119-009-9152-y, 2011.

Ballerine, C.: Topographic wetness index urban flooding awareness act action support, Will & DuPage Counties, Illinois. 2017.

Moore, I. D., Grayson, R. and Ladson, A.: Digital terrain modelling: a review of hydrological, geomorphological, and biological applications. HYDROL PROCESS. 5, 3-30, https://doi.org/10.1002/hyp.3360050103, 1991.

~~1991.~~

~~Pradhan, B., Abokharima, M. H., Jebur, M. N. and Tehrany, M. S.: Land subsidence susceptibility mapping at Kinta Valley (Malaysia) using the evidential belief function model in GIS. NAT HAZARDS. 73, 1019-1042, https://doi.org/10.1007/s11069-014-1128-1~~

~~2014.~~

Azarm, Z., Mehrabi, H. and Nadi, S.: Investigating the Relationship between Subsidence and Groundwater Level Changes using InSAR Time Series Analysis (Isfahan Study Area). Journal of Geography and Environmental Hazards. 11, 173-192, https://doi.org/10.22067/GEOEH.2022.75774.1199, 2023.

~~2023.~~

Neysiani, S. N., Roozbahani, A., Javadi, S. and Shahdany, S. M. H.: Water resources assessment of zayandeh-rood river basin using integrated surface water and groundwater footprints and K-means clustering method. J HYDROL. 614, 128549, https://doi.org/10.1016/j.jhydrol.2022.128549, 2022.

~~2022.~~

Field Code Changed

Formatted: Left

Field Code Changed

Formatted: Left